CHEMISTRY
A EUROPEAN JOURNAL

DOI: 10.1002/chem.200702028

Ultralong Carbon–Carbon Bonds in Dispirobis(10-methylacridan) Derivatives with an Acenaphthene, Pyracene, or Dihydropyracylene Skeleton

Hidetoshi Kawai,*[a, b] Takashi Takeda,[a] Kenshu Fujiwara,[a] Makoto Wakeshima,[a] Yukio Hinatsu,[a] and Takanori Suzuki*[a]

Abstract: Acenapthalene, pyracene, and dihydropyracylene attached to two units of spiroacridan are a novel class of hexaphenylethane (HPE) derivatives that have an ultralong C_{sp^3}–C_{sp^3} bond (1.77–1.70 Å). These sterically challenged molecules were cleanly prepared by C–C bond formation through two-electron reduction from the less-hindered dications. These ultralong bonds were realized based on several molecular-design concepts including enhanced "front strain" through "multiclamping" by means of fusing or bridging aryl groups in the HPE molecule. The lengths of these ultralong bonds and their relation to the conformation (torsional angle) were also validated by means of theoretical calculations. Bond-fission experiments revealed that the bonds are more easily cleaved than standard covalent bonds to produce the corresponding dication upon oxidation with an increase in the length of the C–C bond.

Keywords: crystallography · long bonds · redox chemistry · strained molecules · through-bond interactions

Introduction

Covalent bond lengths, such as 1.54 Å for C_{sp^3}–C_{sp^3}, are basic parameters in chemistry.[1] Compounds that show remarkable deviation from standard values have attracted attention.[2] In addition to the need to elucidate the origin of bond elongation,[3–9] we must also explore novel reactivities that involve such weakened bonds to shed light on the boundary between long bonds and short nonbonds.[10] Because bond energy decreases with an increase in bond length,[11] long bonds are prone to bond fission under homolytic[4,12] or mesolytic[13] conditions. Hexaphenylethane (HPE) derivatives[4] are representative examples in which the polyarylated central C–C bond is elongated, as exemplified by 1,1,2,2-tetraphenylnaphthocyclobutenes,[5] which have a C–C bond length of 1.73 Å. Unlike "cross-clamped" HPE molecules, in which two of the phenyl units are fused or bridged together, "unclamped" HPE molecules, in which the aryl groups are only bonded to the central C–C atoms, are unstable and even the shorter bond (1.65 Å) readily undergoes fission to generate trityl radicals.

In our search for further expanded bonds in stabilized HPE derivatives, we found that the tetraarylacenaphthene skeleton **A** is more promising than that of benzocyclobutene **B** because the former will not suffer from valence isomerization to the bond-dissociated isomer **A′** due to non-Kekulé-type conjugation, whereas the latter is reversibly transformed into the tetraaryl-*o*-quinodimethane **B′**[14] (Scheme 1). Furthermore, we envisaged that the central "ethane" bond of acenaphthene derivative **A** could be longer than that in other HPE-type compounds due to the large interatomic separation between *peri* positions[15–21] of

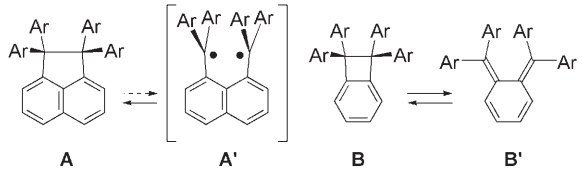

Scheme 1. Schematic formulas for tetraarylacenaphthene **A**, tetraarylbenzocyclobutene **B**, and their bond-dissociated isomers **A′** and **B′**.

[a] Dr. H. Kawai, T. Takeda, Prof. K. Fujiwara, Prof. M. Wakeshima, Prof. Y. Hinatsu, Prof. T. Suzuki
Department of Chemistry, Faculty of Science
Hokkaido University
Kita 10 Nishi 8, Kita-ku, Sapporo 060-0810 (Japan)
Fax: (+81) 11-706-2714
E-mail: kawai@sci.hokudai.ac.jp
tak@sci.hokudai.ac.jp

[b] Dr. H. Kawai
PRESTO, Japan Science and Technology Agency (Japan)

Supporting information for this article is available on the WWW under http://www.chemeurj.org/ or from the author.

the naphthalene ring and the increase of the "front strain"[4b,7b] due to torsional constraints.

Recently, we[19] and Gabbaï et al.[20] independently reported the preparation of some derivatives of **A** that have geometrical features that are consistent with our prediction described above. Herein we report the synthesis and evaluation of acenaphthene **1a** as well as newly prepared pyracene **1b** and dihydropyracylene **1c**. The spiroacridan units are suitable for enhancing geometrical features by further increasing the front strain through "back-clamping", that is, through the substituted aryl rings in general formula **A** being held together by a bridging unit, (Scheme 2). Detailed X-ray structural analyses revealed that these HPE molecules possess some of the longest C–C single bonds ever reported (1.696(3),[19a] 1.707(2)–1.771(3),[19b] and 1.724(3)–1.754(3) Å for **1a**, **1b**, and **1c**, respectively). The nature of these ultralong bonds has been evaluated by theoretical calculations and electrochemical bond-cleavage studies.

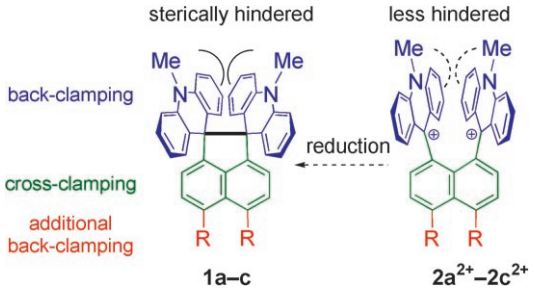

Scheme 2. Generation of dispirobis(10-methylacridan) derivatives **1a–c** (**1a**: R=H; **1b**: R,R=CH_2–CH_2; **1c**: R,R=CH=CH) from the corresponding bis(10-methylacridium) dications $\mathbf{2a}^{2+}$–$\mathbf{2c}^{2+}$.

Results and Discussion

Design and preparation of 1a–c: In our studies on novel electrochromic systems,[22,23] we have found that congested HPE molecules can be easily produced from the corresponding less-hindered bis(diarylmethylium) dications with an arylene spacer by means of a reductive ring-closing reaction.[23] Therefore, we envisaged that sterically challenged dispirobis(10-methylacridan) derivatives **1a–c** could be obtained from dications $\mathbf{2a}^{2+}$–$\mathbf{2c}^{2+}$, in which the acridinium groups are incorporated into the *peri* positions (Scheme 2). Despite the close proximity of the two cationic centers, these dications are less hindered than **1a–c** and can be produced by quaternization of the acridine nitrogen atoms of diacridine compounds **3a–c**.

From the Stille reaction between 1,8-dibromonaphthalene (**4a**)[24] and 9-trimethylstannylacridine (**5**), using [$Pd(PPh_3)_4$] (30 mol%) and CuO (200 mol%) in DMF at 100–140°C,[17] we obtained **3a** in a yield of 23% as slightly soluble yellow crystals (Scheme 3). Under similar conditions, the Stille reactions of 5,6-dibromoacenaphthene (**4b**)[25] and 5,6-dibromoacenaphthylene (**4c**)[26] with **5** gave more-soluble diacridine compounds **3b** and **3c** in higher yields of 48 and 43%, respectively. Upon treatment with a large excess of MeOTf

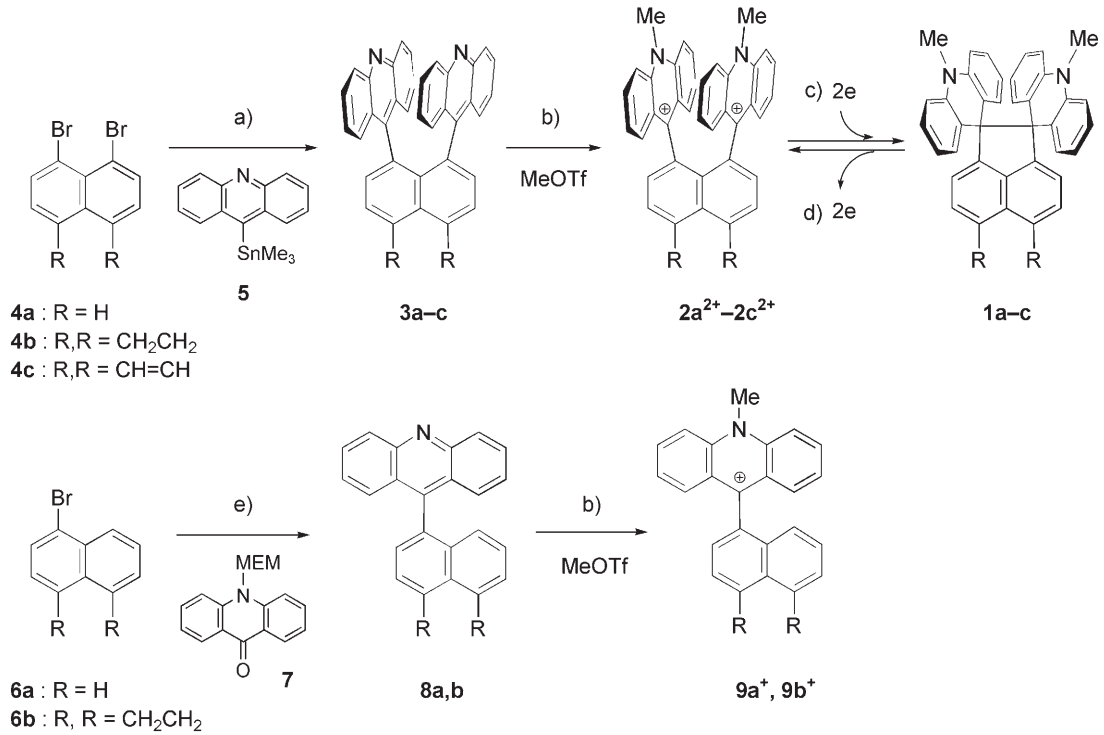

Scheme 3. Preparation of dispirobis(10-methylacridan) derivatives **1a–c** and the reference monocations $\mathbf{9a}^+$ and $\mathbf{9b}^+$. a) **5**, [$Pd(PPh_3)_4$], CuO, DMF, 100–140°C; b) MeOTf, 2,6-di-*tert*-butyl-4-methylpyridine, CH_2Cl_2, 25°C; c) activated Zn in Et_3N/THF for $\mathbf{2a}^{2+}$ and $\mathbf{2b}^{2+}$ or Et_3N/CH_2Cl_2 for $\mathbf{2c}^{2+}$, 25°C; d) [$(4\text{-}BrC_6H_4)_3N$][$SbCl_6$], CH_2Cl_2, 25°C; e) 1. *n*BuLi, **7**, THF, −78°C; 2. HCl_{aq}/EtOH, 25°C.

in the presence of a bulky base (2,6-di-*tert*-butyl-4-methylpyridine) in CH_2Cl_2 at room temperature, compounds **3a–c** were transformed into orange crystals of **2a–c**$[OTf]_2$ salts in yields of 80, 95, and 90%, respectively.

The parallel arrangement of the two acridinium units in $\mathbf{2}^{2+}$ ensures facile C–C bond formation between them upon two-electron reduction. Treatment of **2a**$[OTf]_2$ with Zn in Et_3N/THF (3:10) gave **1a**, a dispiroacenaphthene-type HPE, which was isolated as stable colorless crystals in a yield of 95%. The transformation of $\mathbf{2b}^{2+}$ or $\mathbf{2c}^{2+}$ into **1b** or **1c** also proceeded smoothly under similar conditions, regardless of the longer interatomic distances between the carbenium centers in the dications (see below). Although **1b**,**c** are less stable than **1a** in solution, we could still isolate **1b**,**c** as pale yellow crystals from crude mixtures by careful recrystallization under an inert atmosphere.

Upon reduction, the chemical shifts of the *N*-Me protons of $\mathbf{2a}^{2+}$–$\mathbf{2c}^{2+}$ ($\delta = 4.4$–4.5 ppm in CD_3CN) moved to a higher field ($\delta = 2.61$–2.64 ppm in C_6D_6) in the ^{1}H NMR spectra. The ^{13}C NMR spectra also indicate that the positively charged sp^2-hybridized C9 atom ($\delta = 161.3$, 162.0, and 160.7 ppm for $\mathbf{2a}^{2+}$, $\mathbf{2b}^{2+}$, and $\mathbf{2c}^{2+}$, respectively, in CD_3CN) in $\mathbf{2a}^{2+}$–$\mathbf{2c}^{2+}$ became an uncharged sp^3 carbon atom ($\delta = 70.9$, 75.3, and 76.3 ppm for **1a**, **1b**, and **1c**, respectively, in C_6D_6), which shows that the reduction produced ring-closed HPE molecules **1a–c**.

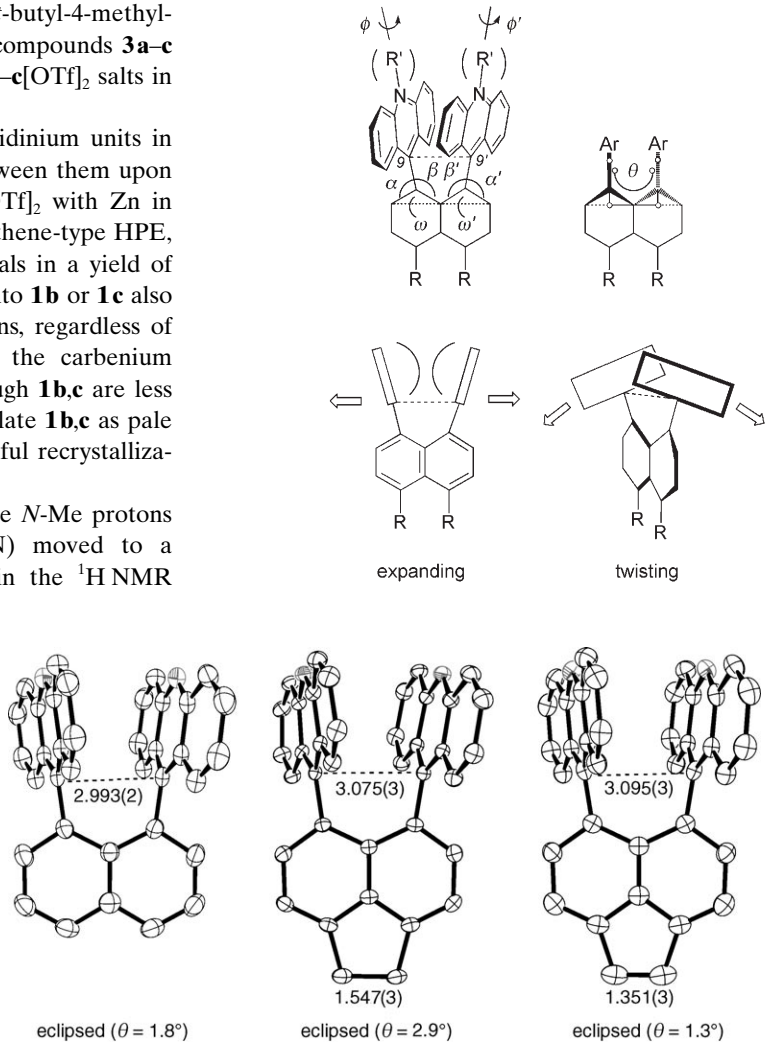

Figure 1. X-ray crystal structures of **3a** (left), **3b** (center), and **3c** (right) (ORTEP representation with 50% probability). Hydrogen atoms are omitted for clarity.

Properties and structures of 3a–c and $\mathbf{2a}^{2+}$–$\mathbf{2c}^{2+}$: Because there are two large π substituents in close proximity at the *peri* position of the naphthalene-type spacer,[16–20] diacridine derivatives **3a–c** and bis(10-methylacridinium) dications $\mathbf{2a}^{2+}$–$\mathbf{2c}^{2+}$ are sterically hindered molecules. They avoid steric repulsion in two ways: by expanding the intersubstituent distance on the naphthalene plane ("expanding"), and by off-sliding of the two substituents orthogonally with respect to the naphthalene plane accompanied by an out-of-plane deformation of the naphthalene skeleton ("twisting"). To understand the differences in *peri* interaction caused by the use of different arylene spacer units, that is, naphthalene, acenaphthene, and acenaphthylene, we studied the X-ray structures of diacridine derivatives **3a–c** and bis(10-methylacridinium) dications $\mathbf{2a}^{2+}$–$\mathbf{2c}^{2+}$. The former show a π–π interaction between two acridine rings in close proximity, whereas the latter show electrostatic repulsion between two acridinium units in addition to a π–π interaction.

Diacridines **3a–c** are stable yellow crystalline materials that exhibit yellowish-green fluorescence (see Figure S1 and Table S1 in the Supporting Information). The X-ray structures of diacridine derivatives **3a–c** (Figure 1, Table 1; and Figures S3–S5 in the Supporting Information) revealed a parallel arrangement of the acridine rings, with the closest nonbonded contacts between the two C9 carbon atoms of the acridine units in the expected order (2.993(2), 3.075(3), and 3.095(3) Å for **3a**, **3b**, and **3c**, respectively). These values are much shorter than the sum of the van der Waals radii of C···C (3.40 Å), and are close to the range of those observed in various 1,8-diarylnaphthalenes[16–19] (2.94–3.00 Å) and 5,6-diarylacenaphthenes[21] (3.10–3.12 Å). The arylene spacer is almost planar ($180° - (\omega, \omega') = < \pm 0.6°$) in all cases, and the out-of-plane deviations of the acridine rings are marginal ($\theta = 1.3$ to $2.9°$). Thus, compounds **3a–c** adopt eclipsed conformations. Both acridine rings are rotated nearly perpendicularly relative to the arylene spacer (φ, $\varphi' = 73.6$ to $75.9°$).

Dications $\mathbf{2a}^{2+}$–$\mathbf{2c}^{2+}$ are red crystalline materials and do not emit fluorescence,[27] although 10-methylacridinium is known to be a strong fluorophore[28] (see Figure S2 and

Table 1. Structural data of **3a–c** and $\mathbf{2a}^{2+}$–$\mathbf{2c}^{2+}$ determined by X-ray analyses.

	3a	**3b**	**3c**	**2a**$[OTf]_2$	**2b**$[OTf]_2$	**2c**$[OTf]_2$
C9···C9′ [Å]	2.993(3)	3.075(3)	3.095(3)	3.020(2)	3.065(5)	3.097(4)
N···N′ [Å]	3.817(3)	3.946(3)	3.785(3)	4.229(2)	3.643(4)	3.782(3)
α, α' [°]	115.2(2), 115.2(2)	116.2(2), 117.6(2)	116.5(2), 116.5(2)	115.7(2), 114.2(2)	117.7(3), 115.3(4)	117.8(2), 116.0(2)
β, β' [°]	125.2(2), 125.2(2)	124.7(2), 123.4(2)	124.7(2), 124.7(2)	123.7(2), 124.7(2)	121.9(4), 125.5(3)	123.3(2), 125.0(2)
$180-(\omega, \omega')$ [°]	0.6 (1), −0.6(1)	0.50(10), −0.34(10)	0.14(7), −0.14(7)	1.66(8), −2.74(9)	1.75(18), 1.36(19)	–0.04(14), 0.27(9)
θ [°]	1.8	2.9	1.3	15.0	3.4	2.7
φ, φ' [°]	75.9(1), 75.9(1)	74.9(1), 75.9(1)	73.6(1), 73.6(1)	84.2(1), 85.8(1)	66.3(2), 67.2(2)	71.3(1), 73.3(1)

Table S1 in the Supporting Information). The electron-accepting properties of $\mathbf{2a}^{2+}$–$\mathbf{2c}^{2+}$ ($E_{red} = -0.07$ (irreversible), −0.25 (reversible), and −0.26 V (reversible) for $\mathbf{2a}^{2+}$, $\mathbf{2b}^{2+}$, and $\mathbf{2c}^{2+}$, respectively) are stronger than those of the corresponding monoacridinium cations $\mathbf{8a}^{+}$ and $\mathbf{8b}^{+}$ (−0.57 (reversible) and −0.59 V (reversible) for $\mathbf{8a}^{+}$ and $\mathbf{8b}^{+}$, respectively; see below), which were prepared[29,30] as shown in Scheme 3. These properties clearly show the strong electronic interaction between the two cationic parts in $\mathbf{2}^{+}$. The higher electron affinity in $\mathbf{2a}^{2+}$ suggests closer contact between the two acridinium units than in $\mathbf{2b}^{2+}$ and $\mathbf{2c}^{2+}$ as verified by the X-ray structures of these salts.

X-ray analysis of the dication salt **2a**$[OTf]_2$ demonstrates that the naphthalene-1,8-diyl skeleton in $\mathbf{2a}^{2+}$ forces the two acridinium units into close proximity (3.020(2) Å; Figure 2, Table 1; Figures S6–S8 in the Supporting Information). The two acridinium rings are offset with twisting deformation of the naphthalene nucleus ($180°-(\omega, \omega') = < \pm 2.7°$) and exhibit significant out-of-plane deviation in the opposite direction ($\theta = 15.0°$). Since a similar out-of-plane deviation was also observed in another salt of $\mathbf{2a}^{2+}$ with different counteranions ($\theta = 16.3°$ for **2a**$[SbCl_6]_2$),[19a] the twisted conformation of $\mathbf{2a}^{2+}$ is energetically feasible for dication $\mathbf{2a}^{2+}$ with a naphthalene spacer to avoid electrostatic repulsion between the positive charges at the *peri* position. On the other hand, the out-of-plane deviations of the two acridinium rings are marginal in the X-ray structures of **2b**$[OTf]_2$ and $\mathbf{2c}^{2+}[OTf]_2$ ($\theta' = 3.4$ and 2.7°, respectively), the eclipsed conformations of which are quite similar to those of the precursors **3b**,**c**. These differences can be explained by the torsional constraints in the acenaphthene and acenaphthylene skeletons due to bridging with an ethane or an ethylene chain (back-clamping) at the opposite *peri* position in the naphthalene ring.[21] Consequently, the molecules with an acenaphthene or acenaphthylene spacer have to reduce steric repulsion by expanding the separation between the acridinium units (3.065(5) and 3.097(4) Å in **2b**$[OTf]_2$ and **2c**$[OTf]_2$, respectively). This deformation mode seems to be intrinsically favored in the case of these arylene spacers. These results demonstrate the validity of our molecular-design concept to fine-tune the relative geometries of the acridine rings by back-clamping in the arylene spacer.

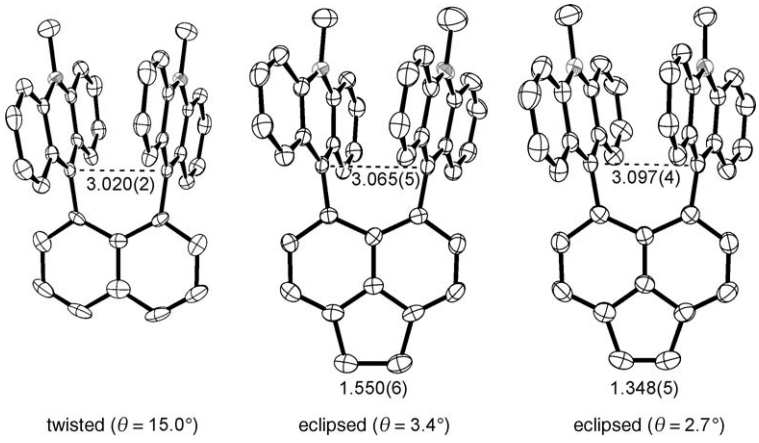

Figure 2. X-ray crystal structures of **2a**$[OTf]_2$ (left), **2b**$[OTf]_2$ (center), and **2c**$[OTf]_2$ (right) (ORTEP representation with 50% probability). Hydrogen atoms and counterions are omitted for clarity.

X-ray structures of molecules 1a–c: Ever since the initial report of very long bonds as revealed by X-ray analyses of 1,1,2,2-tetraarylbenzocyclobutene derivatives,[5] bond lengths greater than 1.70 Å have been acknowledged as "acceptable" values for conventional C_{sp^3}–C_{sp^3} bonds, even though they are significantly longer than the standard (1.54 Å).[5,6,19] Based on the careful examination of thermal ellipsoids for long-bonded atoms or diffraction data at low temperatures, they have been distinguished from crystallographic artifacts and thus proven to be intrinsic.[31] Therefore, we considered that acenaphthene **1a**, pyracene **1b**, and dihydropyracylene **1c** may be promising candidates for exhibiting a greater bond length for several reasons: 1) The "ethane" bond lengths in the parent acenaphthene (calcd[33] at B3LYP/6-31G*: 1.569 Å; exptl: 1.561(8) and 1.552(10) Å in two crystallographically independent molecules[32]), pyracene (calcd: 1.586 Å; exptl: 1.59(3) Å[34]), and dihydropyracylene (calcd: 1.586 Å; no exptl data) are comparable to those in benzocyclobutene (calcd: 1.5816 Å; exptl: 1.576(1) Å[35]) and naphthocyclobutene (calcd: 1.5806 Å; exptl: 1.565(2) Å[36]); 2) The cross-clamping of HPE molecules, by fusing two phenyl units into the naphthalene-type skeleton, plays a role in fixing the substituted aryl groups in almost eclipsed conformations ("torsional constraint"); 3) The back-clamping of HPE mole-

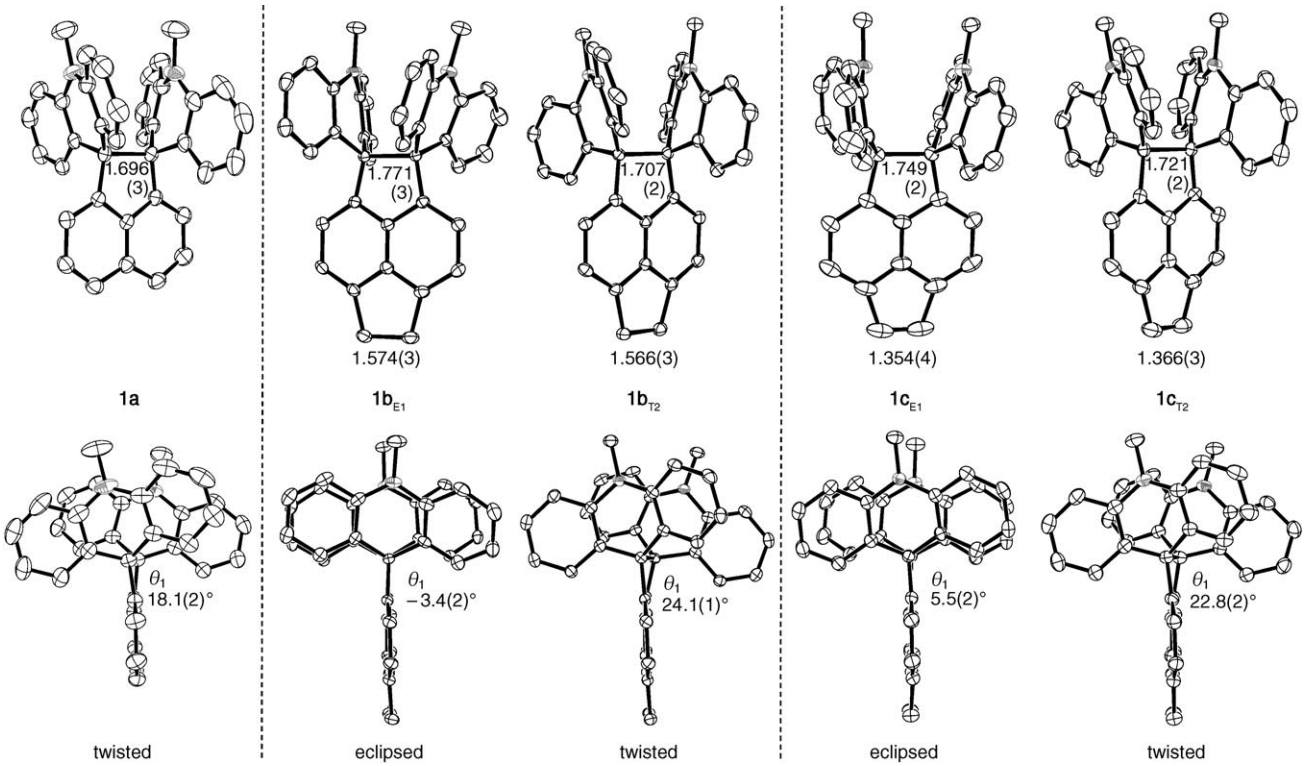

Figure 3. X-ray crystal structures of **1a**, **1b**$_{E1}$, **1b**$_{T2}$, **1c**$_{E1}$, and **1c**$_{T2}$. Top: front view; bottom: side view (ORTEP representation with 50% probability). Hydrogen atoms are omitted for clarity. Two of four (E1, E2, T1, T2) crystallographically independent molecules are shown for **1b**. Two of three (E1, T1, T2) crystallographically independent molecules are shown for **1c**. See Figures S9–S11 in the Supporting Information for X-ray crystal structures of **1b**$_{E2}$, **1b**$_{T1}$, and **1c**$_{T1}$.

cules, by using a spiroacridan unit in place of two phenyl units on the same ethane carbon atom of an HPE molecule, prevents the propeller-shaped geometry of the triphenylmethyl units. This "torsional constraint" induced by the combination of back-clamping and the above-mentioned cross-clamping leads to a highly eclipsed conformation with a larger net front strain; 4) The additional back-clamping in **1b**,**c**, by which the opposite *peri* position was bridged with an ethane (**1b**) or an ethylene unit (**1c**), expands the interatomic distance between the substituents at the *peri* positions (i.e., the C_{sp^3}–C_{sp^3} bond length),[21] and the increased planarity and skeletal rigidity induced by the bridge enhances the preference for the eclipsed conformation in **1b**,**c** by preventing the twisting deformation of the arylene spacers. The validity of molecular-design concepts (2)–(4) was verified by analyzing the detailed X-ray structures of **3a–c** and **2a**$^{2+}$–**2c**$^{2+}$ (see above).

X-ray analysis of dispirobis(10-methylacridan) derivatives **1a–c** revealed that the central C–C bonds are extremely long, as designed (Figure 3 and Table 2). The C1–C2 bond length (d_1) in acenaphthene **1a** was found to be 1.696(3) Å,[19a] which is 0.16 and 0.13 Å longer than the standard value (C_{sp^3}–C_{sp^3}: 1.54 Å) and the corresponding bond in the parent acenaphthene, respectively. The large inner torsion angle ($\theta_1 = \sphericalangle$C8a-C1-C2-C2a) in the acenaphthene skeleton (18.1(2)°) is indicative of the twisted arrangement of the substituents in **1a**, although the out-of-plane deviation of the naphthalene ring is marginal (180−(ω, ω') = 0.5, −0.1°). Thus, cross-clamping by adopting an acenaphthene skeleton cannot completely prevent the twisted deformation as in **2a**$^{2+}$. All of the flanking bond lengths (d_2 and d_3; C1–C(Ar) and C2–C(Ar): 1.509(3)–1.520(4) Å) are similar to or marginally longer than the standard value (C_{sp^2}–C_{sp^3}: 1.51 Å). These results clearly show that the bond elongation observed in the C1–C2 bond is mainly caused by steric factors although the π–σ* through-bond interaction cannot be completely ruled out (see below).

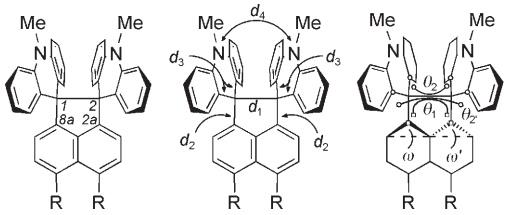

A single high-quality crystal of pyracene **1b** was obtained by recrystallization from a concentrated solution of **1b** in EtOAc. X-ray structural analysis at −180°C gave precise geometrical data with sufficient accuracy (estimated standard deviation (esd) < 0.003 Å),[19b] despite the fact that the crystal contained four crystallographically independent molecules (Figure 3; Figures S9 and S10 in the Supporting Infor-

Table 2. Structural data of **1a–c** determined by X-ray analyses.

	1a[a]	**1b**[b]				**1c**[c]		
		E1	E2	T1	T2	E1	T1	T2
d_1 [Å]	1.696(3)	1.771(3)	1.758(3)	1.712(2)	1.707(2)	1.749(2)	1.726(2)	1.721(2)
d_2 [Å]	1.518(3)	1.521(2)	1.524(2)	1.524(2)	1.525(2)	1.526(3)	1.519(3)	1.522(3)
	1.520(3)	1.523(2)	1.526(2)	1.533(2)	1.533(3)	1.528(2)	1.520(3)	1.534(2)
d_3 [Å]	1.509(3)	1.503(2)	1.510(2)	1.508(2)	1.505(3)	1.509(3)	1.508(2)	1.514(3)
	1.510(4)	1.514(2)	1.511(2)	1.508(3)	1.510(2)	1.512(3)	1.510(3)	1.514(3)
	1.512(3)	1.514(3)	1.511(2)	1.522(2)	1.527(2)	1.518(3)	1.518(2)	1.515(3)
	1.516(4)	1.515(2)	1.513(2)	1.528(2)	1.533(2)	1.518(3)	1.530(3)	15(3)
d_4 [Å]	3.317(3)	3.200(2)	3.192(2)	3.299(2)	3.307(2)	3.159(2)	3.298(2)	3.255(2)
θ_1 [°]	18.1(2)	−3.4(2)	9.4(2)	23.4(1)	24.7(1)	5.5(2)	21.3(2)	22.8(2)
θ_2, $\theta_{2'}$ [°]	23.9(3)	−3.7(2)	12.9(2)	31.5(2)	32.5(2)	6.3(2)	29.5(2)	29.3(2)
	26.0(3)	−6.3(2)	14.5(2)	32.1(2)	34.3(2)	9.0(2)	30.2(2)	30.4(2)
$180-(\omega, \omega')$ [°]	0.5(1)	0.59(8)	0.97(8)	1.93(7)	1.88(7)	0.2(1)	0.64(8)	1.76(9)
	−0.1(1)	−1.02(7)	−0.88(8)	−0.69(6)	−0.73(7)	−0.31(8)	−1.20(9)	−1.02(9)

[a] At −120 °C. [b] At −180 °C. [c] At −130 °C.

mation). They were classified into two categories: the eclipsed conformers $\mathbf{1b}_{E1}$ and $\mathbf{1b}_{E2}$ (inner torsion angle $\theta_1 = -3.4(2)$ and 9.4(2)°, respectively), and the twisted conformers $\mathbf{1b}_{T1}$ and $\mathbf{1b}_{T2}$. Despite the increased rigidity of the five-membered ring fused with the acenaphthene unit, molecules $\mathbf{1b}_{T1}$ and $\mathbf{1b}_{T2}$ adopt a significantly twisted conformation with inner torsion angles (θ_1) of 23.4(1) and 24.7(1)°, respectively. This observation suggests that the eclipsed structure becomes preferred to that in **1a** by incorporating the rigid pyracene skeleton in **1b**, although the twisting deformation could not be completely suppressed. The central C1–C2 bond lengths are 1.712(2) and 1.707(2) Å in $\mathbf{1b}_{T1}$ and $\mathbf{1b}_{T2}$, respectively, which are slightly longer than that in **1a** with a similar twisted conformation. Notably, the two spiroacridan units in $\mathbf{1b}_{E1}$ and $\mathbf{1b}_{E2}$, which are almost eclipsed, suffer from much more severe front strain, which must result in the exceptionally large values of d_1 (1.771(3) and 1.758(3) Å for $\mathbf{1b}_{E1}$ and $\mathbf{1b}_{E2}$, respectively). These values represent the longest C–C bond length ever reported, as distinguished from crystallographic artifacts. Despite their ultralong nature, these bonds can be defined as ordinary covalent bonds, as shown by the electron density (D) maps (Figure 4). If we also consider the tetrahedral geometry for carbon atoms joined by a long bond, the contribution from the bond-dissociated diradical is negligible, at least in the crystal at this temperature. Based on the flanking bond lengths (d_2 and d_3; 1.503(2)–1.526(2) Å for $\mathbf{1b}_{E1}$ and $\mathbf{1b}_{E2}$, and 1.505(3)–1.533(3) Å for $\mathbf{1b}_{T1}$ and $\mathbf{1b}_{T2}$), through-bond coupling[8] is not a decisive reason for the observed bond elongation. The scattering plots of d_1 against θ_1 for the four independent molecules show a negative correlation (Figure 5), which indicates that the greater front strain between the two spiroacridan units in $\mathbf{1b}_{E1}$ and $\mathbf{1b}_{E2}$ is an important factor that accounts for further expansion of the central C–C bond compared with $\mathbf{1b}_{T1}$ and $\mathbf{1b}_{T2}$.

Dihydropyracylene **1c** forms a solvate crystal, $(\mathbf{1c})_3$·EtOAc·0.5 hexane, that does not effloresce and was sufficiently stable under the standard conditions for X-ray data collection. This crystal contains three crystallographically independent molecules with different conformations,

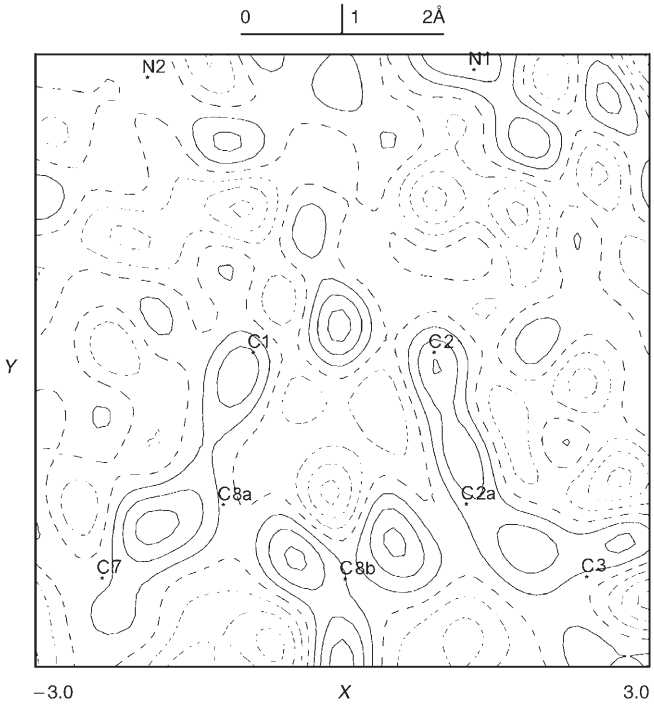

Figure 4. Difference electron-density map (D map) around the ultralong bond in pyracene $\mathbf{1b}_{E1}$ measured at −180 °C. The contour interval is 0.05 e Å^{-3} with the solid lines as positive and the dotted lines as zero and negative.

as in the case of **1b** (Figure 3; Figure S11 in the Supporting Information). One is the eclipsed conformer $\mathbf{1c}_{E1}$ with a longer bond ($d_1 = 1.749(2)$ Å; $\theta_1 = 5.5(2)$°), and the other two are the twisted conformers $\mathbf{1c}_{T1}$ and $\mathbf{1c}_{T2}$ with shorter bonds ($d_1 = 1.726(2)$ and 1.721(2) Å; $\theta_1 = 21.3(2)$ and 22.8(2)°, respectively). Plots of d_1 against θ_1 are located in nearly the same region as those for **1b** (Figure 5). The flanking bond lengths (d_2 and d_3) are close to the standard value (1.509(3)–1.528(2) Å for $\mathbf{1c}_{E1}$, and 1.508(2)–1.534(2) Å for $\mathbf{1c}_{T1}$ and $\mathbf{1c}_{T2}$).

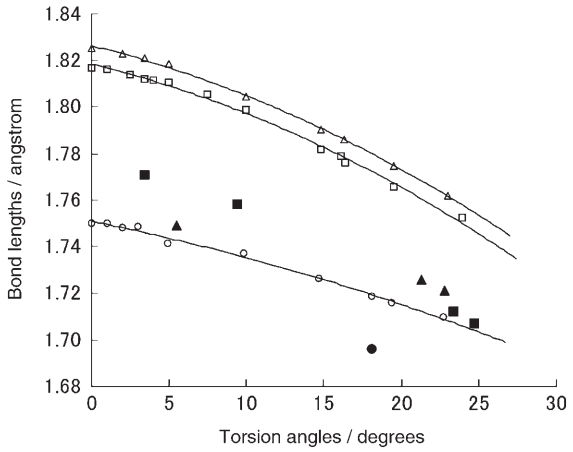

Figure 5. Scattering plots of d_1 versus θ_1 (● for **1a**, ■ for **1b**, and ▲ for **1c**) from X-ray data (all of the conformational isomorphs of **1b,c** are included), and negative correlation in the scattering plots (○ for **1a**, □ for **1b**, and △ for **1c**) for various conformers of **1a–c** optimized at a fixed torsion angle at the B3LYP/6-31G* level.

Theoretical validation of ultralong bonds in 1a–c and dependence of bond lengths on torsion angle: To validate the ultralong bonds in **1a–c** and to elucidate the origin of this elongation, we performed theoretical calculations for **1a–c**. The geometric parameters in **1a–c** calculated at the B3LYP/6-31G* level are in good agreement with the experimental data (Table 3; Table S2 in the Supporting Information), although much longer lengths are predicted for the ultralong C1–C2 bond lengths (d_1 = 1.719, 1.776, and 1.786 Å for **1a**, **1b**, and **1c**, respectively). The twisted form was predicted to be the lowest energy structure in **1a–c** (θ_1 = 18.1, 16.4, and 16.4° for **1a**, **1b**, and **1c**, respectively), however, the eclipsed form (θ_1 = 0°) is also an energy-minimized structure. The attached dispirobis(10-methylacridan) units cause elongation of the central C–C bond of the parent acenaphthene, pyracene, and dihydropyracylene, and the degree of expansion increases in the order 0.150, 0.191, and 0.200 Å for **1a**, **1b**, and **1c**, respectively. These results indicate that a longer bond is prone to expand more easily, which is consistent with the assumption that "the effect of a perturbation on the bond length is larger for an already elongated bond than for a 'normal' bond", as noted by the groups of Ōsawa[8c] and von R. Schleyer.[8e]

Through-bond coupling,[8] that is, the mixing of "lone p" or π orbitals through the intervening σ skeleton, was previously proposed to be one of the possible origins of C–C bond elongation. Orbital-coefficient contours of the HOMO of **1a–c** clearly demonstrate the participation of through-bond coupling (Figure 6; Figure S12 in the Supporting Information); the HOMO consists of π_s–σ orbitals, in which the bonding σ orbital of the long C–C bond is mixed with the π_s orbitals facing each other. The next low-lying orbital, HOMO−1, consists of $\pi_a+\sigma^*$ orbitals, but the mixing of the antibonding σ* orbital seems almost negligible. These results indicate that a filled–filled interaction makes a more important contribution.[9a] When a ($\pi_a+\sigma^*$)-type interaction is responsible for C–C bond elongation, the flanking bonds are expected to be shortened. However, the calculated lengths for the flanking bonds are in the range of 1.516–1.531 Å, and longer than the standard C_{sp^2}–C_{sp^3} bond length (1.51 Å).[1] These results suggest that the orbital interaction is more important in determining the electronic structures of **1a–c** than in affecting their geometrical features.

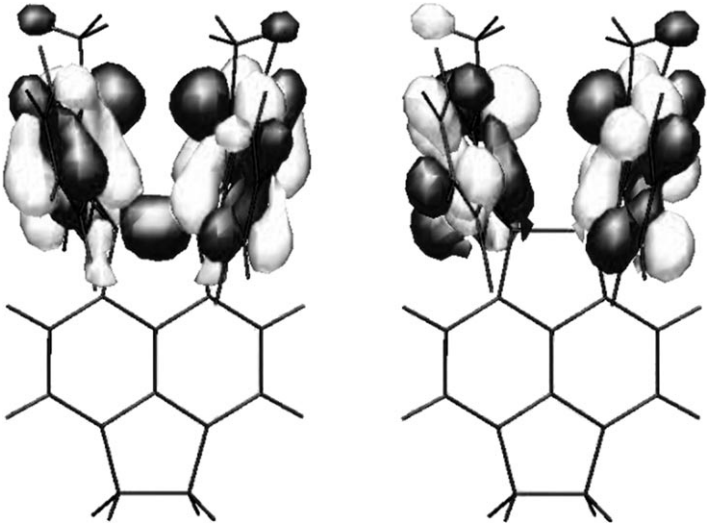

Figure 6. HOMO (left) and HOMO−1 (right) of **1b** calculated at the B3LYP/6-31G* level.

Table 3. Structural data of **1a–c** and related compounds calculated by using the DFT technique (B3LYP/6-31G*).

Compounds	θ_1 [°]	d_1 [Å]	ΔE [kcal mol^{-1}][c]
acenaphthene **1a**	0[a]	1.750	1.09
	5[a]	1.741	1.01
	10[a]	1.737	0.42
	18.1[b]	1.719	–
	23[a]	1.710	0.17
pyracene **1b**	0[a]	1.817	0.78
	5[a]	1.811	0.76
	10[a]	1.799	0.28
	16.4[b]	1.776	–
	24[a]	1.752	0.48
dihydropyracylene **1c**	0[a]	1.825	0.80
	5[a]	1.819	0.77
	10[a]	1.804	0.28
	16.4[b]	1.786	–
	23[a]	1.762	0.47
acenaphthene	0[b]	1.569	–
pyracene	0[b]	1.585	–
dihydropyracylene	0[b]	1.586	–

[a] Optimized with the fixed torsion angle. [b] Full optimization. [c] Relative energy based on the global-minimized structure.

The negative correlation between the ultralong bond length d_1 and the torsion angle (e.g., θ_1 = ∢C8a-C1-C2-C2a) is a key observation that suggests that front strain is the most important factor as the origin of the bond elongation

in HPE molecules **1a–c** (Figure 5). Among the conformational isomorphs in the crystal of **1b**, the longest bond (d_1 = 1.771(3) Å) was found in $\mathbf{1b}_{E1}$, which adopts the most eclipsed conformation ($\theta_1 = -3.4(2)°$) with the greatest front strain, whereas the most twisted conformer $\mathbf{1b}_{T2}$ (θ_1 = 24.7(1)°) with the least front strain exhibits the smallest value for d_1 (1.707(2) Å). This is also the case for the conformational isomorphs of **1c**. In general, conformational isomorphs differ considerably in torsion angles, but not in bond lengths, because the modification of bond lengths requires much more energy than the modification of torsional angles.[19b] Hence, the observed coexistence of isomorphs with a different bond length in **1b**,**c** suggests that the change in the expansion of the C–C bond requires only a small energy difference provided by adopting different packing arrangements in the crystal ("expandability" of the ultralong C–C bond).

To validate this explanation of bond elongation, we undertook the structural optimization of **1a–c** by fixing the torsion angle at a variety of values from 0 to 24° (from an eclipsed form to a twisted form) at the B3LYP/6-31G* level. Figures 5 and 7 show plots of the central C–C bond length and

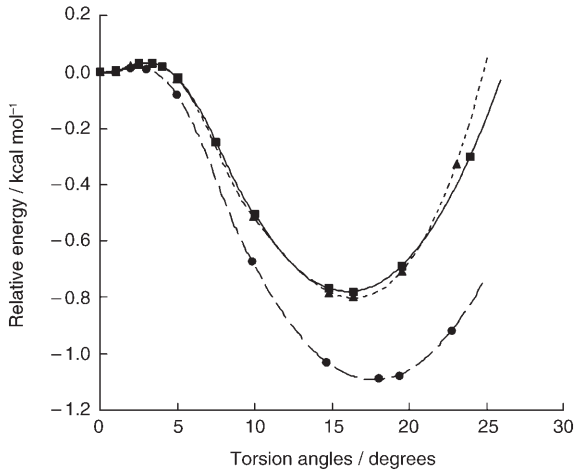

Figure 7. Scattering plots of relative energies ΔE versus θ_1 (● for **1a**; ■ **1b**; ▲ for **1c**) for various conformers of **1a–c** optimized at a fixed torsion angle at the B3LYP/6-31G* level. Global minimized structures were obtained by means of full optimization.

relative energy against the inner torsion angle, respectively. As expected, the central C–C bond elongates as the torsion angle decreases (1.752 Å at 24° to 1.817 Å at 0° for **1b**). Interestingly, the negative slopes in **1b**,**c** are steeper than that in **1a** (Figure 5), which indicates that the elongated bonds of **1b**,**c** can be further expanded by a smaller decrease in torsion angle than in the case of **1a**. Furthermore, each HPE (**1a–c**) exhibits two energy minima at an inner torsion angle of 0 and 16 to 18° (Figure 7), although the potential curve of the eclipsed conformer (θ = 0°) is rather shallow. Although the twisted form is still the conformation with the lowest energy as with other back-clamped HPE molecules, the energy differences between the two conformers are very small in **1a–c** ($\Delta E = -1.09$, -0.78, and -0.80 kcal mol^{-1} for **1a**, **1b**, and **1c**, respectively). Thus, we confirmed that the ultralong C–C bond in **1a–c** can be further elongated by the addition of as little as 1 kcal mol^{-1}. Furthermore, for **1b**,**c** larger differences in bond length are predicted for the two energy-minimized structures (Δd = 0.041 and 0.039 Å for **1b** and **1c**, respectively) than for **1a** (Δd = 0.031 Å), which is consistent with the assumption that the elongated bond can be further expanded by a small input of energy. Consequently, the longest bond in **1b** must be caused by the larger front strain due to the torsional constraint effect from additional back-clamping, as well as by ring strain in the parent skeleton.

Attempted detection of bond-dissociated diradicals by using ESR spectroscopy: In the following sections, we describe the properties and reactivities of **1a–c** that are related to fission of the extremely long bond. To obtain information on the homolytic rupture of the extremely long bond of **1b** to generate the diradical **10b**••, we performed ESR measurements using crystalline samples and a solution of **1b** in benzene. We anticipated that signals assignable to the triplet state of ^{3}**10b**•• would be observed at a higher temperature when the bond-dissociated species (^{1}**10b**••) was present. No signal was observed in solution. In the measurement using polycrystalline samples sealed under an argon atmosphere, only a single sharp resonance appeared at g = 2.0042 at room temperature, which was weakened when the temperature was raised to 120 °C. No other signals were observed. When the sample was cooled, the signal became much weaker. This irreversible temperature dependence suggests that the observed signal is due to a thermally unstable impurity, such as an alkoxy radical (RO•) formed from **1b** upon contact with O_2 before measurement. We observed no evidence to indicate the presence of triplet diradical ^{3}**10b**••,[37] although a contribution from the singlet diradical ^{1}**10b**•• could not be completely ruled out.

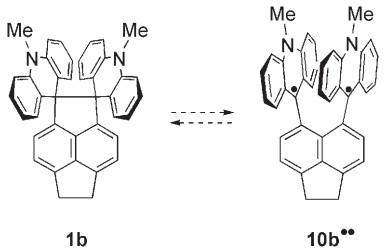

Redox properties of 1a–c and reversible interconversion with $\mathbf{2a}^{2+}$–$\mathbf{2c}^{2+}$: As with other electron-donating HPE molecules,[22,23] the oxidation of **1a–c** is accompanied by cleavage of the long C–C bond ("dynamic redox" property). Thus, the dication salt of $\mathbf{2a}^{2+}$ was regenerated in a yield of 85% upon treatment of **1a** with two equivalents of [(4-$BrC_6H_4)_3N$][$SbCl_6$]. When constant-current electrolyses of the redox pairs **1a**,**1b** and $\mathbf{2a}^{2+}$,$\mathbf{2b}^{2+}$ were followed by using

UV-visible spectroscopy, we found that these redox pairs behave as electrochromic materials, which show reversible interconversion with vivid color changes from colorless to orange. The color change between **1c** and $\mathbf{2c}^{2+}$ is not as clear owing to the presence of the yellow acenaphthylene chromophore. The presence of several isosbestic points in the spectra indicates that these pairs undergo clean electrochemical transformations with negligible steady-state concentrations of the intermediate cation radicals during two-electron transfer. The very low concentrations of the open-shell species is one of the characteristics of electrochromic systems based on dynamic redox systems.

Voltammetric analysis revealed that HPE molecules **1a–c** exhibit very strong electron-donating properties. The oxidation potentials of **1b**,**c** are significantly lower than that of **1a** (E_{ox} = +0.14 (irreversible) −0.25 (reversible), and −0.26 V (reversible) for **1a**, **1b**, and **1c**, respectively) (Table 4; Figure S13 in the Supporting Information). Such differences can be accounted for by considering that the elongated C–C bond has a higher σ-orbital level. Thus, the orbital interaction of the (π_s–σ)-type raises the HOMO level to a larger degree in **1b**,**c** than in **1a**.

Table 4. Table of redox potentials[a] for **1a–c**, $\mathbf{2a}^{2+}$–$\mathbf{2c}^{2+}$, and $\mathbf{9a,b}^{+}$.

Compounds	E_{ox} [V]	E_{red} [V]
redox pair **1a**/$\mathbf{2a}^{2+}$	+0.14	−0.07
redox pair **1b**/$\mathbf{2b}^{2+}$	−0.25	−0.25
redox pair **1c**/$\mathbf{2c}^{2+}$	−0.26	−0.26
monocation $\mathbf{9a}^{+}$	–	−0.57
monocation $\mathbf{9b}^{+}$	–	−0.59

[a] Measured in MeCN containing 0.1 M Et_4NClO_4 (Pt electrode, scan rate 100 mVs^{-1}).

Reactivities of 1a–c toward Brønsted acids: Acenaphthene **1a** is stable and remained intact in the presence of acetic acid in CD_3CN. However, it reacted slowly to generate dication $\mathbf{2a}^{2+}$ when two equivalents of trifluoroacetic acid or *p*-toluenesulfonic acid were added (Scheme 4). As suggested by Gabbaï et al.,[20a] the acid-promoted fission might proceed, if possible, by means of the direct protonation of the long C–C bond. However, in the argon-purged solvent, transformation of **1a** to $\mathbf{2a}^{2+}$ did not occur under otherwise similar conditions, which suggested that the molecular oxygen plays an important role in the bond fission. Pyracene **1b** was converted into dication $\mathbf{2b}^{2+}$ upon treatment with acetic acid in the aerated solvent in accordance with the higher donating properties of **1b** than **1a**.

To prove the reaction mechanism, the time course was followed by using NMR spectroscopy. Figure 8 shows the spectral changes for the reaction of **1a** with *p*-toluenesulfonic acid. The intensity of the peaks for **1a** decreased with an increase in those of $\mathbf{2a}^{2+}$. The NMR spectroscopic investigation of the reaction of **1b** gave similar results, although considerable line broadening was observed in the middle of the reaction course. During the conversion, no peaks assignable to the C–H-bridged carbocations[38] $\mathbf{11a}^{+}$, $\mathbf{11b}^{+}$ or $\mathbf{12a}^{+}$, $\mathbf{12b}^{+}$ were observed in the NMR spectra in both cases, despite the fact that the bridged cations convert to the corresponding dications much slower under similar conditions. We concluded that molecular oxygen acts as an oxidant, and conversion of HPE molecules **1a**,**b** into the corresponding dications $\mathbf{2a}^{2+}$, and $\mathbf{2b}^{2+}$ proceeds via cationic radical species (Scheme 4). Brønsted acids enhance the oxidizing ability of molecular oxygen by protonation of the anion radical after electron transfer.[39] Although we observed fission of the long bond by Brønsted acids as weak as acetic acid, such reactivity is not directly related to the extreme bond length,

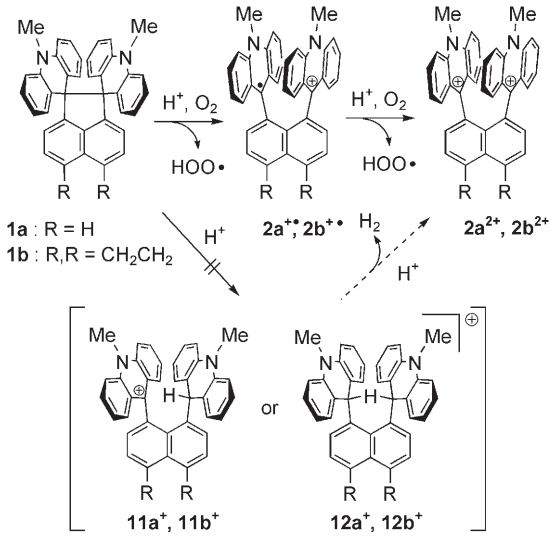

Scheme 4. Plausible reaction mechanism for the bond fission of **1a**,**b** by Brønsted acid.

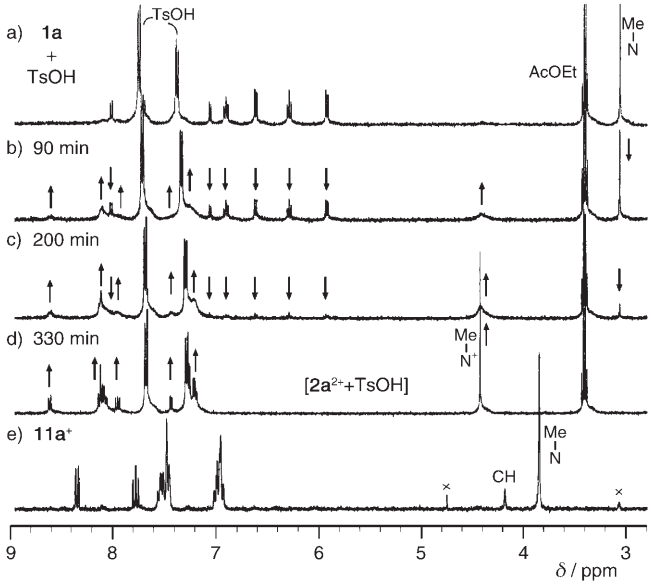

Figure 8. Time course of the NMR spectral change upon treatment of **1a** with TsOH (5 equiv) in CD_3CN at 20 °C at a) 0, b) 90, c) 200, and d) 330 min after the addition of TsOH, and that of e) $\mathbf{11a}^{+}$ prepared by an alternative synthetic method, for comparison.[38]

but is due to the strong donating properties of the molecules, which are enhanced by the bond expansion through the π_s–σ orbital interaction.

Conclusion

We have reported herein the synthesis and evaluation of acenaphthene **1a** as well as newly prepared pyracene **1b** and dihydropyracylene **1c** derivatives that contain spiroacridan units with enhanced geometrical features due to a further increase in front strain by back-clamping of the substituted aryl rings in the HPE. These compounds each possess one of the longest C–C single bonds ever reported (1.696(3), up to 1.771(3), and up to 1.754(3) Å for **1a**, **1b**, and **1c**, respectively). In particular, the central C–C bonds in **1b** and **1c** are substantially elongated relative to **1a**, due to both the increased front strain caused by the additional torsional constraint effect (additional back-clamping) and the intrinsically wide separation between the *peri* positions in the pyracene (**1b**) or the dihydropyracylene (**1c**) spacer. The validity of these effects that cause bond elongation was supported by theoretical calculations. Electrochemical oxidation or acid-promoted oxidation in air induced fission of the very long bonds in **1a–c** to give $\mathbf{2a}^{2+}$–$\mathbf{2c}^{2+}$. However, these compounds are rather stable in the presence of reducing reagents, which indicates that the ultralong bond itself is not so fragile. As shown by the theoretical calculations, further expansion of the long bond requires relatively small amounts of energy. Further studies toward the design and generation of new HPE molecules with much longer C–C bonds are now in progress.

Experimental Section

General: ^{1}H and ^{13}C NMR spectra were recorded on a JEOL AL300 or ECP-300 (^{1}H: 300 MHz; ^{13}C: 75 MHz) spectrometer at 23 °C. The chemical shifts of the ^{1}H and ^{13}C NMR signals are quoted relative to TMS in $CDCl_3$, or to the residual solvent in CD_3CN, [D_8]THF or C_6D_6. IR spectra were taken on a JASCO model FTIR-230 infrared spectrophotometer. Mass spectra were recorded on JEOL JMS-600H (EI, 70 eV); JMS-AX500 or JEOL JMS-SX102A (FAB, 6 keV); and JMS-01SG-2 (FD) spectrometers. Column chromatography was performed on silica gel I-6-40 (YMC) of particle size 40–63 μm and standardized aluminum oxide 90 (Merck 63–200 μm). Melting points were measured on a Yamato MP-21 apparatus. Elemental analyses were taken on a Yanako MT-6 CHN corder at the Center for Instrumental Analysis of Hokkaido University. UV/Vis spectra were recorded on a Hitachi U-3500 spectrophotometer. Fluorescence spectra were recorded on a Hitachi F-4500 spectrofluorometer. ESR spectra were recorded on a JEOL JES-RE1XE X-band spectrometer. 9,9′-(Naphthalene-1,8-diyl)diacridine (**3a**),[38] 9,9′-(acenaphthene-5,6-diyl)diacridine (**3b**),[38] 9,9′-(acenaphthylene-5,6-diyl)diacridine (**3c**),[38] 1,8-dibromonaphthalene (**4a**),[24] 5,6-dibromoacenaphthene (**4b**),[25] 5,6-dibromoacenaphtylene (**4c**),[26] 9-trimethylstannylacridine (**5**),[38] *N*-(2-methoxyethoxymethyl)-9-acridone (**7**),[30] and 10-methyl-9-[6-(10-methylacridan-9-yl)acenaphthen-5-yl]acridinium triflate (**11b**-[OTf])[38] were prepared following known procedures. All commercially available compounds were used without further purification unless otherwise indicated. Solvents were purified prior to use. Reactions were carried out under an argon atmosphere unless otherwise indicated.

Compound 2a[OTf]$_2$: Methyl triflate (600 μL, 5.3 mmol) was added to a mixture of diacridine **3a**[38] (41.5 mg, 86 μmol) and 2,6-di-*tert*-butyl-4-methylpyridine (23.4 mg, 114 μmol) in dry CH_2Cl_2 (2 mL). After stirring for 22 h at 23 °C under argon, the mixture was diluted with diethyl ether and the resulting precipitates were filtered and washed with diethyl ether to give a mixture of **2a**[OTf]$_2$ and pyridinium triflate. This mixture was recrystallized from acetonitrile/diethyl ether to give **2a**[OTf]$_2$ as orange crystals that were large enough to be manually separated under a microscope (56 mg, 80 %) from the colorless crystals of the pyridinium salt. M.p. 258–260 °C (decomp); ^{1}H NMR (CD_3CN): δ = 8.62 (dd, J = 8.4, 1.2 Hz, 2H), 8.10 (ddd, J = 9.4, 5.4, 1.7 Hz, 4H), 8.07 (dd, J = 9.4, 2.1 Hz, 4H), 7.95 (dd, J = 8.4, 7.0 Hz, 2H), 7.44 (dd, J = 7.0, 1.2 Hz, 2H), 7.28 (dd, J = 8.5, 1.7 Hz, 4H), 7.21 (ddd, J = 8.5, 5.4, 2.1 Hz, 4H), 4.42 ppm (s, 6H); ^{13}C NMR (CD_3CN): δ = 161.27, 140.41, 140.00, 135.81, 133.18, 132.28, 132.16, 130.20, 129.73, 129.44, 127.24, 126.87, 119–117, 39.39 ppm; IR (KBr): $\tilde{\nu}$ = 1610, 1551, 1264, 1221, 1143, 1027, 634 cm^{-1}; LR- and HRMS spectra are identical to those of **2a**[$SbCl_6$]$_2$; elemental analysis calcd (%) for $C_{40}H_{28}N_2O_6F_6S_2$: C 59.25, H 3.48, N 3.46; found: C 59.08, H 3.58, N 3.49.

Diacridinium species **2b**[OTf]$_2$ and **2c**[OTf]$_2$ were prepared in a similar manner from **3b**[38] and **3c**,[38] respectively.

Compound 2b[OTf]$_2$: Yield 96 %; orange crystals; m.p. 188–192 °C (decomp); ^{1}H NMR (CD_3CN): δ = 8.17 (br d, J = 9.3 Hz, 4H), 8.04 (dd, J = 9.3, 6.6, 1.5 Hz, 4H), 7.77 (d, J = 7.2 Hz, 2H), 7.44 (dd, J = 8.7, 1.5 Hz, 4H), 7.43 (d, J = 7.2 Hz, 2H), 7.22 (ddd, J = 8.7, 6.6, 0.9 Hz, 4H), 4.50 (s, 6H), 3.79 ppm (s, 4H); ^{13}C NMR (CD_3CN): δ = 162.02, 152.11, 140.93, 140.20, 140.13, 133.93, 130.89, 130.6 (br), 129.09, 126.85, 125.09, 124.24, 121.29, 39.37, 31.35 ppm; IR (KBr): $\tilde{\nu}$ = 1605, 1579, 1548, 1284, 1263, 1251, 1224, 1152, 1029, 769, 755, 636 cm^{-1}; UV/Vis (CH_3CN): λ_{max} (ε) = 232 (76400), 253 (123000), 352 (15400), 426 nm (8000 M^{-1}cm^{-1}); LRMS (FAB): m/z (%): 538 (24) [M^+], 523 (15), 307 (35), 289 (22); HRMS (FAB): m/z calcd for $C_{38}H_{24}N_2$: 538.2409; found: 538.2403; elemental analysis calcd (%) for $C_{42}H_{30}N_2O_6F_6S_2$: C 60.28, H 3.61, N 3.35; found: C 59.71, H 3.80, N 3.84.

Compound 2c[OTf]$_2$: Yield 90 %; orange crystals; m.p. 155–156 °C (decomp); ^{1}H NMR (CD_3CN): δ = 8.17 (br d, J = 9.4 Hz, 4H), 8.11 (d, J = 7.2 Hz, 2H), 8.06 (ddd, J = 9.4, 6.6, 1.3 Hz, 4H), 7.50 (d, J = 7.2 Hz, 2H), 7.50 (dd, J = 8.5, 1.3 Hz, 4H), 7.49 (s, 2H), 7.22 (ddd, J = 8.5, 6.6, 1.3 Hz, 4H), 4.51 ppm (s, 6H); ^{13}C NMR (CD_3CN): δ = 160.73, 143.84, 140.24, 140.09, 133.65, 132.44, 130.88, 130.33, 130.15, 129.88, 129.24, 127.79, 126.70, 125.74, 39.50 ppm; IR (KBr): $\tilde{\nu}$ = 3115, 1609, 1580, 1549, 1460, 1379, 1265, 1224, 1193, 1153, 1032, 874, 759, 636, 517 cm^{-1}; UV/Vis (CH_3CN): λ_{max} (ε) = 235 (73900), 253 (147000), 354 (20700), 426 nm (11100 M^{-1}cm^{-1}); LRMS (FAB): m/z (%): 685 (33), 537 (47), 536 (69) [M^+], 535 (40), 522 (45); HRMS (FAB): m/z calcd for $C_{40}H_{28}N_2$: 536.2242; found: 536.2260; elemental analysis calcd (%) for $C_{42}H_{28}N_2O_6F_6S_2 + CH_3CN$: C 60.34, H 3.57, N 4.80; found: C 60.15, H 3.68, N 4.56.

Compound 1a: Activated Zn powder (126 mg, 1.9 mmol) was added to a suspension of **2a**[OTf]$_2$ (39.3 mg, 49 μmol) in dry Et_3N/THF (3:10, 13 mL), and the mixture was stirred for 38 h at 23 °C. The mixture was diluted with water and extracted with EtOAc. The organic layer was washed with brine and dried over Na_2SO_4. After filtration, an orange solid was obtained by evaporation of the solvent and was subjected to chromatography on Al_2O_3 eluting with CH_2Cl_2/*n*-hexane (1:1) to give **1a** as a white solid (24 mg, 95 %). M.p. 265–266 °C (decomp); ^{1}H NMR ($CDCl_3$): δ = 7.95 (dd, J = 8.3, 0.6 Hz, 2H), 7.68 (dd, J = 8.3, 6.9 Hz, 2H), 7.17 (dd, J = 6.9, 0.6 Hz, 2H), 6.92 (ddd, J = 8.3, 7.2, 1.4 Hz, 4H), 6.59 (dd, J = 8.3, 0.8 Hz, 4H), 6.33 (ddd, J = 7.8, 7.2, 0.8 Hz, 4H), 6.04 (dd, J = 7.8, 1.4 Hz, 4H), 3.08 ppm (s, 6H); ^{13}C NMR ($CDCl_3$): δ = 147.15, 141.16, 140.87, 130.29, 129.56, 129.06, 126.66, 126.43, 124.41, 123.82, 118.68, 110.36, 70.57, 32.96 ppm; IR (KBr): $\tilde{\nu}$ = 2924, 1590, 1474, 1358, 1274, 1133, 1055, 784, 747, 700 cm^{-1}; UV/Vis (CH_3CN): λ_{max} (ε) = 215 (84500), 298 nm (24300 M^{-1}cm^{-1}); LRMS (EI): m/z (%): 513 (41), 512 (100) [M^+], 498 (41), 497 (97); HRMS (FAB): m/z calcd for $C_{38}H_{28}N_2$: 512.2252; found: 512.2250; elemental analysis calcd (%) for $C_{38}H_{28}N_2$: C 88.68, H 5.88, N 5.44; found: C 88.97, H 5.68, N 5.41.

Compound 1b: Activated Zn powder (479 mg, 7.3 mmol) was added to a suspension of **2b**$[OTf]_2$ (44.0 mg, 53 μmol) in dry Et_3N/THF (3:10, 13 mL), and the mixture was stirred for 63 h at 23 °C. The mixture was diluted with water and extracted with CH_2Cl_2. The organic layer was washed with brine and then dried over Na_2SO_4. After filtration, the orange solid obtained by evaporation of the solvent was purified by recrystallization from EtOAc/*n*-hexane under an inert atmosphere to give **1b** as pale yellow crystals (13.2 mg, 47 %). M.p. 150–151 °C (decomp); ^{1}H NMR ([D$_8$]THF): δ = 7.43 (d, J = 7.0 Hz, 2H), 7.01 (d, J = 7.0 Hz, 2H), 6.83 (ddd, J = 8.0, 7.4, 1.4 Hz, 4H), 6.55 (d, J = 8.0 Hz, 4H), 6.24 (dd, J = 7.7, 7.4 Hz, 4H), 6.04 (dd, J = 7.7, 1.4 Hz, 4H), 3.64–3.58 (m, 4H), 3.10 ppm (s, 6H); ^{13}C NMR ([D$_8$]THF): δ = 143.29, 142.92, 142.25, 140.67, 138.37, 130.21, 127.32, 127.27, 126.17, 122.61, 119.20, 111.23, 75.64, 33.30, 32.61 ppm; IR (KBr): $\tilde{\nu}$ = 2922, 2851, 1474, 1470, 1261, 1238, 1157, 1101, 1045, 803, 744 cm^{-1}; LRMS (EI): *m*/*z* (%): 539 (42), 538 (77) [M^+], 524 (53), 523 (100), 278 (27), 269 (44); HRMS (FAB): *m*/*z* calcd for $C_{40}H_{30}N_2$: 538.2409; found: 538.2412.

Compound 1c: Zn powder (187 mg, 2.9 mmol) was added to a suspension of **2c**$[OTf]_2$ (43.3 mg, 52 μmol) in dry Et_3N/CH_2Cl_2 (3:10, 26 mL), and the mixture was stirred for 37 h at 23 °C. The mixture was diluted with water and extracted with CH_2Cl_2. The organic layer was washed with brine and dried over Na_2SO_4. After filtration, the orange solid obtained by evaporation of the solvent was purified by recrystallization from EtOAc/*n*-hexane under an inert atmosphere to give **1c** as pale yellow crystals (4.5 mg, 16 %). M.p. 150–151 °C (decomp); ^{1}H NMR (C_6D_6): δ = 7.65 (d, J = 7.0 Hz, 2H), 7.23–7.09 (m, 4H), 6.87 (d, J = 6.7 Hz, 4H), 6.36–6.26 (m, 12H), 2.62 ppm (s, 6H); ^{13}C NMR (C_6D_6): δ = 148.52, 141.50, 137.24, 137.01, 130.12, 129.87, 129.14, 128.75, 128.32, 127.05, 126.70, 125.75, 119.32, 110.75, 76.31, 31.91 ppm; IR (KBr): $\tilde{\nu}$ = 2960, 2926, 2855, 2365, 2340, 1608, 1592, 1475, 1466, 1455, 1428, 1358, 1274, 1168, 1132, 1053, 868, 844, 747, 688, 652 cm^{-1}; LRMS (EI): *m*/*z* (%): 537 (46), 536 (91) [M^+], 522 (91), 521 (100); HRMS (EI): *m*/*z* calcd for $C_{40}H_{28}N_2$: 536.2252; found: 536.2256.

Oxidation of HPE 1a to dication 2a[SbCl$_6$]$_2$: $[(4\text{-}BrC_6H_4)_3N][SbCl_6]$ (84 mg, 103 μmol) was added to a solution of **1a** (24 mg, 46 μmol) in dry CH_2Cl_2, and the mixture was stirred for 2.5 h at 23 °C under argon. The resulting precipitates were filtered and washed with CH_2Cl_2 to give **2a**-$[SbCl_6]_2$ as an orange solid (47 mg, 86 %). M.p. 255–258 °C (decomp); ^{1}H NMR and ^{13}C NMR spectra are identical to those of **2a**$[OTf]_2$; IR (KBr): $\tilde{\nu}$ = 2924, 1590, 1474, 1358, 1274, 1133, 1055, 784, 747, 700 cm^{-1}; UV/Vis (CH_3CN): λ_{max} (ε) = 224 (76300), 253 (145000), 355 (17300), 427 nm (7200 M^{-1}cm^{-1}); LRMS (FAB): *m*/*z* (%): 512 (100) [M^+]; HRMS (FAB): *m*/*z* calcd for $C_{38}H_{28}N_2$: 512.2252; found: 512.2262; elemental analysis calcd (%) for $C_{38}H_{28}N_2$: C 88.68, H 5.88, N 5.44; found: C 88.97, H 5.68, N 5.41.

Compound 8a: At −78 °C under argon, *n*BuLi in *n*-hexane (1.54 M, 5.0 mL, 7.8 mmol) was added dropwise to a solution of 1-bromonaphthalene (**6a**; 1.0 mL, 7.1 mmol) in dry THF (20 mL). After 20 min, a solution of *N*-(2-methoxyethoxymethyl)-9-acridone (**7**)[30] (1.20 g, 4.2 mmol) in dry THF (30 mL) was added dropwise. The mixture was allowed to warm to 23 °C and was stirred for 23 h at this temperature. The mixture was diluted with water and extracted with $CHCl_3$. The organic layer was washed with brine. The yellow solid obtained by evaporation of the solvent was dissolved in a mixture of EtOH and 2 M aqueous HCl (1:1, 100 mL), and the mixture was stirred for 15 h at 23 °C. The resulting solution was neutralized with 2 M aqueous NaOH and extracted with CH_2Cl_2. The combined organic layer was washed with brine and dried over Na_2SO_4. After filtration, the yellow solid obtained by evaporation of the solvent was subjected to chromatography on silica gel eluting with $CHCl_3/Et_3N$ (100:1) to give **8a** as a yellow solid (625 mg, 48 %). M.p. 237.0–237.5 °C; ^{1}H NMR ($CDCl_3$): δ = 8.33 (d, J = 8.8 Hz, 2H), 8.09 (d, J = 8.3 Hz, 1H), 8.01 (d, J = 8.3 Hz, 1H), 7.77 (ddd, J = 8.8, 6.6, 1.1 Hz, 2H), 7.69 (dd, J = 8.3, 6.9 Hz, 1H), 7.50 (d, J = 6.8 Hz, 1H), 7.49 (dd, J = 8.3, 7.9 Hz, 1H), 7.44 (dd, J = 8.8, 1.1 Hz, 2H), 7.32 (dd, J = 8.8, 6.6 Hz, 2H), 7.23 (dd, J = 8.3, 7.9 Hz, 1H), 7.02 ppm (d, J = 8.3 Hz, 1H); ^{13}C NMR ($CDCl_3$): δ = 164.08, 160.98, 148.91, 148.74, 147.85, 145.35, 144.93, 144.15, 143.70, 143.59, 142.20, 141.91, 141.52, 141.34, 141.27, 141.00, 140.56 ppm; IR (KBr): $\tilde{\nu}$ = 1558, 1545, 1515, 1506, 1461, 1436, 1391, 1011, 804, 798, 782, 768, 752, 619, 604 cm^{-1}; UV/Vis (CH_2Cl_2): λ_{max} (ε) = 281 (7700), 292 (5400, sh), 342 (6900, sh), 360 (11000), 385 nm (5900 M^{-1}cm^{-1}); fluorescence (CH_2Cl_2, λ_{ex} = 360 nm): λ_{max} = 425 nm; LRMS (EI): *m*/*z* (%): 306 (45), 305 (100) [M^+], 304 (66), 303 (37); HRMS (EI): *m*/*z* calcd for $C_{23}H_{15}N$: 305.1204; found: 305.1208; elemental analysis calcd (%) for $C_{23}H_{15}N$: C 90.46, H 4.95, N 4.59; found: C 90.21, H 5.01, N 4.57.

Acridine **8b** was prepared in a similar manner from 5-bromoacenaphthene (**6b**).

Compound 8b: Yield 43 %; yellow solid; m.p. 209.0–209.5 °C; ^{1}H NMR ($CDCl_3$): δ = 8.32 (d, J = 8.8 Hz, 2H), 7.77 (ddd, J = 8.8, 6.6, 1.5 Hz, 2H), 7.54 (dd, J = 8.8, 0.7 Hz, 2H), 7.50–7.45 (m, 2H), 7.32 (ddd, J = 8.8, 6.6, 1.5 Hz, 2H), 7.26–7.20 (m, 2H), 3.57 ppm (s, 4H); ^{13}C NMR ($CDCl_3$): δ = 148.87, 147.05, 146.26, 145.80, 139.23, 131.10, 130.26, 130.04, 129.63, 128.79, 128.53, 127.11, 126.09, 125.53, 120.99, 119.80, 118.93, 30.59, 30.36 ppm; IR (KBr): $\tilde{\nu}$ = 3054, 2916, 2836, 1607, 1514, 1011, 838, 756, 605 cm^{-1}; UV/Vis (CH_2Cl_2): λ_{max} (ε) = 254 (126000), 342 (7000, sh), 358 (11000), 386 nm (6800 M^{-1}cm^{-1}); fluorescence (CH_2Cl_2, λ_{ex} = 360 nm): λ_{max} = 458 nm; LRMS (EI): *m*/*z* (%): 332 (26), 331 (100) [M^+], 330 (47), 328 (25); HRMS (EI): *m*/*z* calcd for $C_{25}H_{17}N$: 331.1361; found: 331.1361, elemental analysis calcd (%) for $C_{25}H_{17}N$: C 90.60, H 5.17, N 4.23; found: C 90.41, H 5.33, N 4.31.

Preparation of 9a[OTf]: Methyl triflate (2.0 mL, 17.7 mmol) was added to a solution of **8a** (625 mg, 2.0 mmol) in dry CH_2Cl_2 (10 mL). After stirring for 13 h at 23 °C under argon, the mixture was diluted with diethyl ether. The resulting precipitates were filtered and washed with diethyl ether to give **9a**[OTf] as an orange solid (693 mg, 72 %). M.p. 226–228 °C (decomp); ^{1}H NMR: (CD_3CN): δ = 8.64 (br d, J = 9.3 Hz, 2H), 8.36 (ddd, J = 9.3, 6.3, 1.9 Hz, 2H), 8.30 (dd, J = 8.3, 1.3 Hz, 1H), 8.15 (dd, J = 8.1, 1.3 Hz, 1H), 7.83 (dd, J = 8.3, 7.0 Hz, 1H), 7.77 (dd, J = 8.8, 1.9 Hz, 2H), 7.72 (dd, J = 8.8, 6.3 Hz, 2H), 7.61 (dd, J = 7.0, 1.3 Hz, 1H), 7.59 (ddd, J = 8.1, 7.0, 0.7 Hz, 1H), 7.32 (ddd, J = 8.4, 7.0, 1.3 Hz, 1H), 6.94 (dd, J = 8.4, 0.7 Hz, 1H), 4.88 ppm (s, 3H); ^{13}C NMR (CD_3CN): δ = 161.82, 142.72, 139.85, 134.40, 132.93, 131.65, 131.51, 130.90, 129.67, 129.54, 128.96, 128.55, 127.98, 127.93, 126.38, 126.11, 119.61, 39.78 ppm; IR (KBr): $\tilde{\nu}$ = 1610, 1581, 1551, 1272, 1222, 1160, 1030, 809, 781, 759, 636, 517 cm^{-1}; UV/Vis (CH_3CN): λ_{max} (ε) = 222 (85200), 261 (98300), 344 (8800, sh), 361 nm (19800 M^{-1}cm^{-1}, sh); LRMS (FAB): *m*/*z* (%): 320 (93) [M^+], 185 (95), 93 (100), 75 (56); HRMS (FAB): *m*/*z* calcd for $C_{24}H_{18}N$: 320.1434; found: 320.1422; elemental analysis calcd (%) for $C_{25}H_{18}NO_3F_3S$: C 63.96, H 3.86, N 2.98; found: C 63.86, H 4.04, N 2.93.

Acridinium **9b**[OTf] was prepared in a similar manner from 5-bromoacenaphthene (**8b**).

Compound 9b[OTf]: Yield 73 %; orange solid; m.p. 257–258 °C (decomp); ^{1}H NMR (CD_3CN): δ = 8.64 (d, J = 9.4 Hz, 2H), 8.36 (ddd, J = 9.4, 6.6, 1.6 Hz, 2H), 7.86 (ddd, J = 8.6, 1.6, 0.7 Hz, 2H), 7.73 (ddd, J = 8.6, 6.6, 0.7 Hz, 2H), 7.64 (d, J = 6.9 Hz, 1H), 7.55 (d, J = 6.9 Hz, 1H), 7.41 (d, J = 6.9 Hz, 1H), 7.32 (dd, J = 8.4, 6.9 Hz, 1H), 6.68 (d, J = 8.4 Hz, 1H), 4.87 (s, 3H), 3.61–3.55 ppm (m, 4H); ^{13}C NMR (CD_3CN): δ = 162.15, 150.65, 148.03, 142.71, 139.83, 139.76, 131.59, 131.56, 131.00, 130.60, 128.77, 128.00, 126.79, 121.58, 120.65, 120.04, 119.60, 39.72, 31.13 ppm (2C); IR (KBr): $\tilde{\nu}$ = 3047, 2919, 1605, 1580, 1550, 1446, 1389, 1362, 1267, 1224, 1194, 1144, 1029, 843, 789, 767, 637, 572, 516 cm^{-1}; UV/Vis (CH_3CN): λ_{max} (ε) = 229 (66300), 260 (84000), 345 (8000, sh), 361 (17800), 423 nm (5100 M^{-1}cm^{-1}); LRMS (FAB): *m*/*z* (%): 347 (77), 346 (100) [M^+], 345 (28), 344 (32); HRMS (EI): *m*/*z* calcd for $C_{26}H_{20}N$: 346.1590; found: 346.1586; elemental analysis calcd (%) for $C_{27}H_{20}NO_3F_3S$: C 65.45, H 4.07, N 2.83; found: C 65.37, H 4.23, N 2.78.

Bond fission of 1a,b by Brønsted acids: Brønsted acid was added to a solution of **1** (0.40 mg, 0.78 mmol) in aerated CD_3CN (0.6 mL) in an NMR tube. The time course of the bond-fission reaction and consumption of **1** were monitored by using ^{1}H NMR spectroscopy. In the case of **1a**-TsOH, conversion to $\mathbf{2a}^{2+}$ was completed 330 min after addition. When the deaerated solvent was used, compound **1** remained intact without forming $\mathbf{2}^{2+}$.

Redox potential measurements: Redox potentials (E_{ox} and E_{red}) were measured by using cyclic voltammetry with samples in dry MeCN containing 0.1 M Et_4NClO_4 as a supporting electrolyte. Ferrocene undergoes one-electron oxidation at +0.38 V under the same conditions. All of the

values shown in the text are in E [V] versus SCE measured at the scan rate of 100 mV s^{-1}. Platinum disk electrodes were used as the working and counter electrodes. The working electrode was polished by using a suspension of Al_2O_3 in water (0.05 μm) before use. The irreversible half-wave potentials were estimated from the anodic peak potentials (E_{pa}) as $E_{ox} = E_{pa} - 0.03$ or the cathodic peak potentials (E_{pc}) as $E_{red} = E_{pa} + 0.03$.

Computational methods: The DFT calculations were performed with the Gaussian 98 program package.[33] The geometries of the compounds were optimized by using the B3LYP method[39] in combination with the 6-31G* basis set without performing frequency calculations. The structural optimizations for **1a–c** were also carried out with the torsion angle fixed at several values in the range of 0 to 24° (from an eclipsed form to a twisted form) by using the keywords "Opt=ModRedundant" and "Constants: R=(torsion angle)" at the B3LYP/6-31G* level.

X-ray analyses

General: The data were obtained by using a Rigaku Mercury charge-coupled device (CCD) apparatus ($Mo_{K\alpha}$ radiation, $\lambda = 0.71070$ Å). A numerical absorption correction (μ) was applied. The structures were solved by direct methods and refined by the full-matrix least-squares method on F^2 with anisotropic temperature factors for non-hydrogen atoms. All the hydrogen atoms were located at the calculated positions and refined with riding. The esd values of the bond lengths (C–C) and angles (∢) are also given.

*Crystal data for **1a***: Crystals were obtained by recrystallization from CH_2Cl_2/hexane. $C_{38}H_{28}N_2$; $M_r = 512.65$; colorless prism; crystal size 0.20×0.10×0.05 mm^3; monoclinic; space group $P2_1/n$; $a = 10.415(5)$, $b = 18.582(8)$, $c = 13.744(6)$ Å; $\beta = 102.120(10)°$; $V = 2600.5(20)$ Å^3; $Z = 4$; $\rho = 1.309$ g cm^{-1}; $\mu = 0.76$ cm^{-1}; 5676 reflections measured; 390 parameters; 5676 unique reflections ($2\theta_{max} = 55°$; $T = 153$ K); direct method SIR92 used; $R1 = 0.057$ ($I > 2\sigma I$); $wR2 = 0.146$ (all data); esd(C–C) 0.003–0.005 Å; esd(∢) 0.2–0.3°; CCDC-651845.

*Crystal data for **1b***: Crystals were obtained by recrystallization from EtOAc. $C_{40}H_{30}N_2$; $M_r = 538.69$; pale yellow block; crystal size 0.60×0.60×0.35 mm^3; triclinic; space group $P\bar{1}$; $a = 17.699(3)$, $b = 18.111(3)$, $c = 18.844(3)$ Å; $\alpha = 111.183(2)$, $\beta = 93.828(1)$, $\gamma = 102.130(2)°$; $V = 5438.5(14)$ Å^3; $Z = 8$; $\rho = 1.316$ g cm^{-1}; $\mu = 0.76$ cm^{-1}; 23025 reflections measured; 1633 parameters; 23025 unique reflections ($2\theta_{max} = 55°$; $T = 93$ K); direct method SIR92 used; $R1 = 0.052$ ($I > 2\sigma I$); $wR2 = 0.120$ (all data); esd(C–C) 0.002–0.003 Å; esd(∢) 0.1–0.2°; CCDC-651843.

*Crystal data for (**1c**)$_3$·EtOAc·0.5 hexane*: Crystals were obtained by recrystallization from EtOAc/hexane. $(C_{40}H_{28}N_2)_3 \cdot C_4H_8O_2 \cdot 0.5\,(C_6H_{14})$; $M_r = 1741.22$; yellow block; crystal size 0.60×0.20×0.05 mm^3; triclinic; space group $P\bar{1}$; $a = 16.327(2)$, $b = 16.582(3)$, $c = 17.190(3)$ Å; $\alpha = 103.212(3)$, $\beta = 90.271(2)$, $\gamma = 96.274(2)°$; $V = 4501.3(12)$ Å^3; $Z = 2$; $\rho = 1.285$ g cm^{-1}; $\mu = 0.76$ cm^{-1}; 19777 reflections measured; 1316 parameters; 19777 unique reflections ($2\theta_{max} = 55°$; $T = 143$ K); direct method SIR97 used; $R1 = 0.068$ ($I > 2\sigma I$); $wR2 = 0.149$ (all data); esd(C–C) 0.003–0.02 Å; esd(∢) 0.2–1°; CCDC-632944.

*Crystal data for **2a**[OTf]$_2$*: Crystals were obtained by recrystallization from MeCN/diethyl ether. $C_{38}H_{28}N_2(CF_3SO_3)_2$; $M_r = 810.78$; brown block; crystal size 0.65×0.45×0.25 mm^3; monoclinic; space group $P2_1/n$; $a = 17.602(4)$, $b = 10.715(2)$, $c = 19.766(4)$ Å; $\beta = 112.712(3)°$; $V = 3439.0(12)$ Å^3; $Z = 4$; $\rho = 1.566$ g cm^{-1}; $\mu = 2.42$ cm^{-1}; 7540 reflections measured; 599 parameters; 7537 unique reflections ($2\theta_{max} = 55°$; $T = 153$ K); direct method SIR97 used; $R1 = 0.045$ ($I > 2\sigma I$); $wR2 = 0.107$ (all data); esd(C–C) 0.001–0.003 Å; esd(∢) 0.08–0.2°; CCDC-651844.

*Crystal data for [**2b**]$_2$[OTf]$_4$·MeCN*: Crystals were obtained by recrystallization from MeCN/diethyl ether. $(C_{40}H_{30}N_2)_2(CF_3SO_3)_4 \cdot C_2H_3N$; $M_r = 1714.69$; red platelet; crystal size 0.70×0.10×0.03 mm^3; triclinic; space group $P\bar{1}$; $a = 12.0911(7)$, $b = 12.6996(7)$, $c = 14.9765(11)$ Å; $\alpha = 69.925(13)$, $\beta = 67.336(11)$, $\gamma = 64.697(12)°$; $V = 1874.0(3)$ Å^3; $Z = 1$; $\rho = 1.519$ g cm^{-1}; $\mu = 2.27$ cm^{-1}; 8000 reflections measured; 583 parameters; 8000 unique reflections ($2\theta_{max} = 55°$; $T = 153$ K); direct method SIR97 used; $R1 = 0.077$ ($I > 2\sigma I$); $wR2 = 0.227$ (all data); esd(C–C) 0.002–0.017 Å; esd(∢) 0.2–0.6°; CCDC-632945.

*Crystal data for **2c**[OTf]$_2$·MeCN*: Crystals were obtained by recrystallization from MeCN/diethyl ether. $C_{40}H_{28}N_2(CF_3SO_3)_2 \cdot C_2H_3N$; $M_r = 875.86$; red block; crystal size 0.25×0.25×0.25 mm^3; monoclinic; space group $P2_1/c$; $a = 13.273(3)$, $b = 19.666(4)$, $c = 14.832(3)$ Å; $\beta = 93.159(5)°$; $V = 3865.6(14)$ Å^3; $Z = 4$; $\rho = 1.505$ g cm^{-1}; $\mu = 2.23$ cm^{-1}; 8491 reflections measured; 581 parameters; 8491 unique reflections ($2\theta_{max} = 55°$; $T = 113$ K); direct method SIR92 used; $R1 = 0.065$ ($I > 2\sigma I$); $wR2 = 0.147$ (all data); esd(C–C) 0.002–0.008 Å; esd(∢) 0.2–0.6°; CCDC-632946.

*Crystal data for **3a***: Crystals were obtained by recrystallization from $CHCl_3$/hexane. $C_{36}H_{22}N_2$; $M_r = 482.58$; colorless prism; crystal size 0.35×0.15×0.03 mm^3; orthorhombic; space group $Pbcn$; $a = 15.457(4)$, $b = 10.539(3)$, $c = 14.217(4)$ Å; $V = 2316(1)$ Å^3; $Z = 4$; $\rho = 1.384$ g cm^{-1}; $\mu = 0.81$ cm^{-1}; 2540 reflections measured; 184 parameters; 2540 unique reflections ($2\theta_{max} = 55°$; $T = 153$ K); direct method SIR92 used; $R1 = 0.056$ ($I > 2\sigma I$); $wR2 = 0.107$ (all data); esd(C–C) 0.002–0.004 Å; esd(∢) 0.1–0.2°; CCDC-651846.

*Crystal data for **3b***: Crystals were obtained by recrystallization from $CHCl_3$/EtOAc. $C_{38}H_{24}N_2$; $M_r = 508.62$; yellow block; crystal size 0.40×0.25×0.15 mm^3; triclinic; space group $P\bar{1}$; $a = 9.0654(18)$, $b = 11.924(3)$, $c = 12.355(2)$ Å; $\alpha = 77.092(11)$, $\beta = 70.684(11)$, $\gamma = 86.428(14)°$; $V = 1228.4(5)$ Å^3; $Z = 2$; $\rho = 1.375$ g cm^{-1}; $\mu = 0.80$ cm^{-1}; 5212 reflections measured; 385 parameters; 5212 unique reflections ($2\theta_{max} = 55°$; $T = 153$ K); direct method SIR92 used; $R1 = 0.075$ ($I > 2\sigma I$); $wR2 = 0.237$ (all data); esd(C–C) 0.002–0.003 Å; esd(∢) 0.16–0.2°; CCDC-632947.

*Crystal data for **3c***: Crystals were obtained by recrystallization from $CHCl_3$/hexane. $C_{38}H_{22}N_2$; $M_r = 506.61$; yellow block; crystal size 0.20×0.15×0.10 mm^3; orthorhombic; space group $Pbcn$; $a = 15.278(2)$, $b = 11.6399(16)$, $c = 14.0311(19)$ Å; $V = 2495.3(6)$ Å^3; $Z = 4$; $\rho = 1.348$ g cm^{-1}; $\mu = 0.78$ cm^{-1}; 2755 reflections measured; 193 parameters; 2755 unique reflections ($2\theta_{max} = 55°$; $T = 123$ K); direct method SHELX97 used; $R1 = 0.054$ ($I > 2\sigma I$); $wR2 = 0.119$ (all data); esd(C–C) 0.002–0.004 Å; esd(∢) 0.13–0.2°; CCDC-632948.

CCDC-632944, 632945, 632946, 632947, 632948, 651843, 651844, 651845, and 651846 contain the supplementary crystallographic data for this paper. These data can be obtained free of charge from the Cambridge Crystallographic Data Centre via www.ccdc.cam.ac.uk/data_request/cif.

Acknowledgements

This work was supported by Hokkaido University Grant Program for Leading Edge Research, Japan (2005). We thank Prof. Tamotsu Inabe (Hokkaido University) for use of the X-ray structural analysis system and Prof. Masako Kato and Dr. Kiyoshi Tsuge (Hokkaido University) for the solid-state UV-visible spectra measurements. MS spectra were measured by Dr. Eri Fukushi and Mr. Kenji Watanabe at the GC–MS NMR Laboratory (Faculty of Agriculture, Hokkaido University). T.T. gratefully acknowledges financial support from JSPS (18-4425).

[1] a) F. H. Allen, O. Kennard, D. G. Watson, L. Brammer, A. G. Orpen, R. Taylor, *J. Chem. Soc. Perkin Trans. 2* **1987**, *12*, S1–S19; b) L. C. Pauling, *The Nature of the Chemical Bond and the Structure of Molecules and Crystal*, 3rd ed., Cornell University Press, Ithaca, NY, **1960**.

[2] a) H. Hopf, *Classics in Hydrocarbon Chemistry*, Wiley-VCH, Weinheim, **2000**; b) *Advances in Strained and Interesting Organic Molecules* (Ed.: B. Halton), JAI Press, Stamford, Ct, **2000**; c) I. V. Komarov, *Russ. Chem. Rev.* **2001**, 70, 991–1016; d) T. Tsuji in *Modern Cyclophane Chemistry* (Eds.: R. Gleiter, H. Hopf), Wiley-VCH, Weinheim, **2005**, pp. 81–104; e) S. Vázquez, P. Camps, *Tetrahedron* **2005**, *61*, 5147–5208; f) M. Tanaka, A. Sekiguchi, *Angew. Chem.* **2005**, *117*, 5971–5973; *Angew. Chem. Int. Ed.* **2005**, *44*, 5821–5823; g) K. Tani, B. M. Stoltz, *Nature* **2006**, *441*, 731–734.

[3] a) G. Kaupp, J. Boy, *Angew. Chem.* **1997**, *109*, 48–50; *Angew. Chem. Int. Ed. Engl.* **1997**, *36*, 48–49; b) F. Toda, *Eur. J. Org. Chem.* **2000**, 1377–1386.

[4] a) J. M. McBride, *Tetrahedron* **1974**, *30*, 2009–2022; b) W. D. Hounshell, D. A. Dougherty, J. P. Hummel, K. Mislow, *J. Am. Chem. Soc.*

1977, *99*, 1916–1924; c) M. Stein, W. Winter, A. Rieker, *Angew. Chem.* **1978**, *90*, 737–738; *Angew. Chem. Int. Ed. Engl.* **1978**, *17*, 692–694; d) E. Osawa, Y. Onuki, K. Mislow, *J. Am. Chem. Soc.* **1981**, *103*, 7475–7479; e) B. Kahr, D. V. Engen, K. Mislow, *J. Am. Chem. Soc.* **1986**, *108*, 8305–8307; f) N. Yannoni, B. Kahr, K. Mislow, *J. Am. Chem. Soc.* **1988**, *110*, 6670–6672; g) C. R. Arkin, B. Cowans, B. Kahr, *Chem. Mater.* **1996**, *8*, 1500–1503.

[5] a) F. Toda, K. Tanaka, Z. Stein, I. Goldberg, *Acta Crystallogr. Sect. C* **1996**, *52*, 177–180; b) F. Toda, K. Tanaka, M. Watanabe, K. Tamura, I. Miyahara, T. Nakai, K. Hirotsu, *J. Org. Chem.* **1999**, *64*, 3102–3105; c) K. Tanaka, N. Takamoto, Y. Tezuka, M. Kato, F. Toda, *Tetrahedron* **2001**, *57*, 3761–3767; d) F. Toda, K. Tanaka, N. Takamoto, *Tetrahedron Lett.* **2001**, *42*, 7979–7982.

[6] S. Kammermeier, P. G. Jones, R. Herges, *Angew. Chem.* **1997**, *109*, 2317–2319; *Angew. Chem. Int. Ed. Engl.* **1997**, *36*, 1757–1760.

[7] a) T. Suzuki, K. Ono, J. Nishida, H. Takahashi, T. Tsuji, *J. Org. Chem.* **2000**, *65*, 4944–4948; b) T. Suzuki, K. Ono, H. Kawai, T. Tsuji, *J. Chem. Soc. Perkin Trans. 2* **2001**, 1798–1801.

[8] a) D. A. Dougherty, W. D. Hounshell, H. B. Schlegel, R. A. Bell, K. Mislow, *Tetrahedron Lett.* **1976**, *17*, 3479–3482; b) D. A. Dougherty, H. B. Schlegel, K. Mislow, *Tetrahedron* **1978**, *34*, 1441–1447; c) E. Ōsawa, P. M. Ivanov, C. Jaime, *J. Org. Chem.* **1983**, *48*, 3990–3993; d) S. Ōsawa, M. Sakai, E. Ōsawa, *J. Phys. Chem. A* **1997**, *101*, 1378–1383; e) H. F. Bettinger, P. von R. Schleyer, H. F. Schaefer III, *Chem. Commun.* **1998**, 769–770.

[9] a) K. K. Baldridge, T. R. Battersby, R. VernonClark, J. S. Siegel, *J. Am. Chem. Soc.* **1997**, *119*, 7048–7054; b) C. H. Choi, M. Kertesz, *Chem. Commun.* **1997**, 2199–2200; c) K. K. Baldridge, Y. Kasahara, K. Ogawa, J. S. Siegel, K. Tanaka, F. Toda, *J. Am. Chem. Soc.* **1998**, *120*, 6167–6168; d) V. Galasso, I. Carmichael, *J. Phys. Chem. A* **2000**, *104*, 6271–6276; e) R. Isea, *THEOCHEM* **2001**, *540*, 131–138; f) Y. Orimoto, Y. Aoki, *Int. J. Quantum Chem.* **2002**, *86*, 456–467.

[10] a) J. L. Adcock, A. A. Gakh, J. L. Pollitte, C. Woods, *J. Am. Chem. Soc.* **1992**, *114*, 3980–3981; b) R. A. Pascal, Jr., *Eur. J. Org. Chem.* **2004**, 3763–3771.

[11] A. A. Zavitsas, *J. Phys. Chem. A* **2003**, *107*, 897–898.

[12] M. Frenette, C. Aliaga, E. Font-Sanchis, J. C. Scaiano, *Org. Lett.* **2004**, *6*, 2579–2582.

[13] E. M. Arnett, R. A. Flowers II, A. E. Meekhof, L. Miller, *J. Am. Chem. Soc.* **1993**, *115*, 12603–12604.

[14] a) G. Quinkert, W.-W. Wiersdorff, M. Finke, K. Opitz, F.-G. von der Haar, *Chem. Ber.* **1968**, *101*, 2302–2325; b) S. Iwashita, E. Ohta, H. Higuchi, H. Kawai, K. Fujiwara, K. Ono, M. Takenaka, T. Suzuki, *Chem. Commun.* **2004**, 2076–2077; c) S. Iwashita, T. Suzuki, *J. Synth. Org. Chem. Jpn.* **2006**, *64*, 958–968.

[15] a) V. Balasubramaniyan, *Chem. Rev.* **1966**, *66*, 567–641; b) J. D. Hoefelmeyer, M. Schulte, M. Tschinkl, F. P. Gabbaï, *Coord. Chem. Rev.* **2002**, *232*, 93–103.

[16] a) H. O. House, D. G. Koespell, W. J. Campbell, *J. Org. Chem.* **1972**, *37*, 1003–1011; b) W. B. Schweizer, G. Procter, M. Kaftory, J. D. Dunitz, *Helv. Chim. Acta* **1978**, *61*, 2783–2808; c) K. Komatsu, N. Abe, K. Takahashi, K. Okamoto, *J. Org. Chem.* **1979**, *44*, 2712–2717; d) R. Tsuji, K. Komatsu, Y. Inoue, K. Takeuchi, *J. Org. Chem.* **1992**, *57*, 636–641; e) F. Cozzi, M. Cinquini, R. Annuziata, T. Dwyer, J. S. Siegel, *J. Am. Chem. Soc.* **1992**, *114*, 5729–5733; f) F. Cozzi, M. Cinquini, R. Annuziata, J. S. Siegel, *J. Am. Chem. Soc.* **1993**, *115*, 5330–5331; g) J. A. Zoltewicz, N. M. Maier, W. M. F. Fabian, *J. Org. Chem.* **1996**, *61*, 7018–7021; h) T. Katoh, Y. Inagaki, R. Okazaki, *J. Am. Chem. Soc.* **1998**, *120*, 3623–3628; i) P. M. Iovine, M. A. Kellett, N. P. Redmore, M. J. Therien, *J. Am. Chem. Soc.* **2000**, *122*, 8717–8727; j) S. Lavieri, J. A. Zoltewicz, *J. Org. Chem.* **2001**, *66*, 7227–7230; k) C. Wolf, B. T. Ghebremariam, *Tetrahedron: Asymmetry* **2002**, *13*, 1153–1156.

[17] a) C. Wolf, X. Mei, *J. Am. Chem. Soc.* **2003**, *125*, 10651–10658; b) X. Mei, C. Wolf, *J. Org. Chem.* **2005**, *70*, 2299–2305; c) X. Mei, R. M. Martin, C. Wolf, *J. Org. Chem.* **2006**, *71*, 2854–2861.

[18] a) T. Suzuki, T. Nagasu, H. Kawai, K. Fujiwara, T. Tsuji, *Tetrahedron Lett.* **2003**, *44*, 6095–6098; b) H. Kawai, T. Nagasu, T. Takeda, K. Fujiwara, T. Tsuji, M. Ohkita, J. Nishida, T. Tsuji, *Tetrahedron Lett.* **2004**, *45*, 4553–4558.

[19] a) H. Kawai, T. Takeda, K. Fujiwara, T. Suzuki, *Tetrahedron Lett.* **2004**, *45*, 8289–8293; b) H. Kawai, T. Takeda, K. Fujiwara, T. Inabe, T. Suzuki, *Cryst. Growth Des.* **2005**, *5*, 2256–2260.

[20] a) H. Wang, F. P. Gabbaï, *Angew. Chem.* **2004**, *116*, 186–189; *Angew. Chem. Int. Ed.* **2004**, *43*, 184–187; b) H. Wang, C. E. Webster, L. M. Pérez, M. B. Hall, F. P. Gabbaï, *J. Am. Chem. Soc.* **2004**, *126*, 8189–8196; c) H. Wang, F. P. Gabbaï, *Org. Lett.* **2005**, *7*, 283–285.

[21] a) R. L. Clough, W. J. Kung, R. E. Marsh, J. D. Roberts, *J. Org. Chem.* **1976**, *41*, 3603–3609; b) W. Cross, G. E. Hawkes, R. T. Kroemer, K. R. Liedl, T. Loerting, R. Nasser, R. G. Pritchard, M. Steele, M. Watkinson, A. Whiting, *J. Chem. Soc. Perkin Trans. 2* **2001**, 459–467; c) M. Steele, M. Watkinson, A. Whiting, *J. Chem. Soc. Perkin Trans. 1* **2001**, 588–589.

[22] a) J. Nishida, T. Suzuki, T. Tsuji, *J. Synth. Org. Chem. Jpn.* **2002**, *60*, 40–51; b) T. Suzuki, H. Higuchi, T. Tsuji, J. Nishida, Y. Yamashita, T. Miyashi in *Chemistry of Nanomolecular Systems, Chapter 1: Dynamic Redox Systems* (Eds.: T. Nakamura, T. Matsumoto, H. Tada, K. Sugiura), Springer, Heidelberg, **2003**, p. 3; c) H. Highchi, E. Ohta, H. Kawai, K. Fujiwara, T. Tsuji, T. Suzuki, *J. Org. Chem.* **2003**, *68*, 6605–6610; d) E. Ohta, H. Higuchi, H. Kawai, K. Fujiwara, T. Suzuki, *Org. Biomol. Chem.* **2005**, *3*, 3024–3031; e) T. Suzuki, E. Ohta, H. Kawai, K. Fujiwara, T. Fukushima, *Synlett* **2007**, 851–869.

[23] a) T. Suzuki, J. Nishida, T. Tsuji, *Angew. Chem.* **1997**, *109*, 1387–1389; *Angew. Chem. Int. Ed. Engl.* **1997**, *36*, 1329–1331; b) T. Suzuki, J. Nishida, T. Tsuji, *Chem. Commun.* **1998**, 2193–2194; c) J. Nishida, T. Suzuki, M. Ohkita, T. Tsuji, *Angew. Chem.* **2001**, *113*, 3351–3354; *Angew. Chem. Int. Ed.* **2001**, *40*, 3251–3254; d) T. Suzuki, R. Yamamoto, H. Higuchi, E. Hirota, M. Ohkita, T. Tsuji, *J. Chem. Soc. Perkin Trans. 2* **2002**, 1937–1942; e) T. Suzuki, A. Migita, H. Higuchi, H. Kawai, K. Fujiwara, *Tetrahedron Lett.* **2003**, *44*, 6837–6840; f) T. Suzuki, S. Tanaka, H. Higuchi, H. Kawai, K. Fujiwara, *Tetrahedron Lett.* **2004**, *45*, 8563–8567; g) T. Suzuki, S. Tanaka, H. Kawai, K. Fujiwara, *Chem. Asian J.* **2007**, *2*, 171–177; h) T. Suzuki, T. Iwai, E. Ohta, H. Kawai, K. Fujiwara, *Tetrahedron Lett.* **2007**, *48*, 3599–3603; i) T. Suzuki, R. Tamaki, E. Ohta, T. Takeda, H. Kawai, K. Fujiwara, M. Kato, *Tetrahedron Lett.* **2007**, *48*, 3823–3827.

[24] a) H. H. Hodgson, J. S. Whitehurst, *J. Chem. Soc.* **1947**, 80; b) D. Seyferth, S. C. Vick, *J. Organomet. Chem.* **1977**, *141*, 173–187; c) Š. Vyskočil, L. Meca, I. Tišlerová, I. Císařová, M. Polášek, S. R. Harutyunyan, Y. N. Belokon, R. M. J. Stead, L. Farrugia, S. C. Lockhart, W. L. Mitchell, P. Kočovský, *Chem. Eur. J.* **2002**, *8*, 4633–4648.

[25] a) N. Tanaka, T. Kasai, *Bull. Chem. Soc. Jpn.* **1981**, *54*, 3020–3025; b) W. D. Neudorff, D. Lentz, M. Anibarro, A. D. Schlüter, *Chem. Eur. J.* **2003**, *9*, 2745–2757.

[26] R. H. Mitchell, M. Chaudhary, R. V. Williams, R. Fyles, J. Gibson, M. J. Ashwood-Smith, A. J. Fry, *Can. J. Chem.* **1992**, *70*, 1015–1021.

[27] H. van Willingen, G. Jones II, M. S. Farahat, *J. Phys. Chem.* **1996**, *100*, 3312–3316.

[28] S. A. Jonker, F. Ariese, J. W. Verhoeven, *Recl. Trav. Chim. Pays-Bas* **1989**, *108*, 109–115.

[29] H. Koshima, K. Kutsunai, *Heterocycles* **2002**, *57*, 1299–1302.

[30] a) Z. Zeng, S. C. Zimmerman, *Tetrahedron Lett.* **1988**, *29*, 5123–5124; b) S. C. Zimmerman, K. W. Saionz, Z. Zeng, *Proc. Natl. Acad. Sci. USA* **1993**, *90*, 1190–1193; c) T. Tanaka, T. Tasaki, Y. Aoyama, *J. Am. Chem. Soc.* **2002**, *124*, 12453–12462.

[31] The bond in silabicyclobutane might be one of the longest C–C bonds (1.781 Å) ever reported, yet its estimated standard deviation (0.015 Å) is too large to compare the value with other precisely determined bond lengths: G. Fritz, S. Wartanessian, E. Matern, W. Hönle, H. G. von Schnering, *Z. Anorg. Allg. Chem.* **1981**, *475*, 87–108.

[32] A. C. Hazell, R. G. Hazell, L. Nørskov-Lauritsen, C. E. Briant, D. W. Jones, *Acta Crystallogr. Sect. C* **1986**, *42*, 690–693.

[33] Gaussian 98 (Revision A.7), M. J. Frisch, G. W. Trucks, H. B. Schlegel, G. E. Scuseria, M. A. Robb, J. R. Cheeseman, V. G. Zakrzewski, J. A. Montgomery, Jr., R. E. Stratmann, J. C. Burant, S. Dapprich, J. M. Millam, A. D. Daniels, K. N. Kudin, M. C. Strain, O. Farkas, J. Tomasi, V. Barone, M. Cossi, R. Cammi, B. Mennucci, C. Pomelli, C. Adamo, S. Clifford, J. Ochterski, G. A. Petersson, P. Y. Ayala, Q. Cui, K. Morokuma, D. K. Malick, A. D. Rabuck, K. Raghavachari, J. B. Foresman, J. Cioslowski, J. V. Ortiz, B. B. Stefanov, G. Liu, A. Liashenko, P. Piskorz, I. Komaromi, R. Gomperts, R. L. Martin, D. J. Fox, T. Keith, M. A. Al-Laham, C. Y. Peng, A. Nanayakkara, C. Gonzalez, M. Challacombe, P. M. W. Gill, B. G. Johnson, W. Chen, M. W. Wong, J. L. Andres, M. Head-Gordon, E. S. Replogle, J. A. Pople, Gaussian, Inc., Pittsburgh, PA, **1998**.

[34] G. L. Simmons, E. C. Lingafelter, *Acta Crystallogr.* **1961**, *14*, 872–874.

[35] R. Boese, D. Bläser, *Angew. Chem.* **1988**, *100*, 293–295; *Angew. Chem. Int. Ed. Engl.* **1988**, *27*, 304–305.

[36] J. L. Crawford, R. E. Marsh, *Acta Crystallogr. Sect. B* **1973**, *29*, 1238–1241.

[37] Toda et al. reported in ref. [5d] that the long bond in 1,1,2,2-tetraphenylnaphthocyclobutenes was not ruptured either.

[38] a) H. Kawai, T. Takeda, K. Fujiwara, T. Suzuki, *J. Am. Chem. Soc.* **2005**, *127*, 12172–12173; b) T. Takeda, H. Kawai, K. Fujiwara, T. Suzuki, *Chem. Eur. J.* **2007**, *13*, 7915–7925.

[39] a) A. D. Becke, *J. Chem. Phys.* **1993**, *98*, 5648–5652; b) C. Lee, W. Yang, R. G. Parr, *Phys. Rev. B* **1988**, *37*, 785–789; c) B. Miehlich, A. Savin, H. Stoll, H. Preuss, *Chem. Phys. Lett.* **1989**, *157*, 200–206.

Received: December 22, 2007
Published online: May 14, 2008

